

UNIVERSIDADE DE LISBOA
INSTITUTO SUPERIOR TÉCNICO
Università degli Studi di Padova

Tokamak Magnetic Control Simulation: Applications for JT60-SA and ISTTOK Operation.

Doménica Corona Rivera

Supervisor: Prof. Horácio Fernandes

Co-Supervisor: Prof. Nuno Cruz

External supervisor: Prof. Alfredo Pironti

Thesis specifically prepared to obtain the PhD Degree in
Technological Physics Engineering

Month 2020

ABSTRACT

Abstract en ingles

Keywords:Real-time control, plasma current, centroid position, state-space

RESUMO

Abstract em tuga

Palavras-chave:

SOMMARIO

Abstract em italiano

Parole chiave:

ACKNOWLEDGEMENTS

This work was supported by Fundação para a Ciência e a Tecnologia (FCT) under the grant No.**PD/BD/114306/2016** carried out as part of the training in the framework of the Advanced Program in Plasma Science and Engineering (APPLAuSE, sponsored by FCT under grant No. PD/00505/2012).

CONTENTS

1	INTRODUCTION	3
1.1	Tokamak plasma control	3
1.2	Behind the plasma current	3
1.3	Thesis outline	3
2	PLASMA CONTROL SYSTEMS	5
2.1	Overview of control systems	5
2.1.1	DIII-D Plasma Control System	5
2.1.2	Système de Contrôle Distribué	7
2.2	MARTe framework	7
2.2.1	MARTe architecture	8
2.2.2	Hardware containers	8
2.2.3	MARTe 2.0	9
2.3	Equilibrium and control algorithms	9
2.3.1	State-Space models	9
2.3.2	PID control	9
2.3.3	Multiple-Input Multiple-Output control	9
3	JT60-SA CONTROL DESIGN	11
3.1	Machine description	11
3.2	CREATE magnetic reconstruction tools	13
3.3	Controller design	13
3.4	QST reconstruction and control implementation	16
3.4.1	Cauchy Condition Surface reconstruction method	16
3.4.2	QST magnetic controller (FBC)	17
3.5	Simulation results	18
3.5.1	Disturbances	20
3.5.2	Gap-based XSC	20
3.5.3	Isoflux XSC and QST controller	20
3.5.4	Shape reference change	20
4	ISTTOK	23
4.1	Machine description	23
4.2	Diagnostics and Actuators	23
4.3	ATCA-MIMO-ISOL boards	23

Contents

4.3.1	Hardware layout	23
4.3.2	Real-time integration software	23
4.4	Plasma current magnetic field	23
4.5	Plasma centroid position determination	23
5	ISTTOK RESULTS	25
5.1	Implementation of the General Application Modules	25
5.1.1	PID control implementation	25
5.1.2	Data-driven state-space model retrieving	25
5.1.3	Kalman filter implementation	25
5.1.4	Multiple-Input Multiple-Output control implementation	25
5.2	Plasma curruent centroid position control results	25
5.2.1	PID control and LQR control results	31
6	CONCLUSIONS	35
	Bibliography	39
A	EXTENDED CONTROL RESULTS	41
B	FBC CONTROLLER AND CCS CONFIGURATION	55

LIST OF FIGURES

Figure 2.1	DIII-D digital PCS in 1991 [2].	6
Figure 2.2	Actual DIII-D PCS real-time systems [4].	6
Figure 2.3	TCV SCD. Real-time network nodes connection. The nodes configurations are shown together with the typical diagnostic and actuator systems to which they are connected [7].	7
Figure 2.4	Example of a set of GAMs connected to the DDB. Timing and hardware GAMs provide the I/O interface to the exterior, whereas a generic waveform GAM inputs the reference for a PID controller. Finally, the output is sent to a DAC and the data is stored for analysis by a collection GAM. It should be noticed that the reference generation and the controller GAM are not aware of the changes in the data providers and data consumers. [11]	8
Figure 3.1	JT60-SA tokamak configuration and its main elements [15].	11
Figure 3.2	JT-60SA poloidal cross-section and layout of the Poloidal Field coils system [16].	12
Figure 3.3	LCFS Equilibria corresponding to the different Scenario 2 snapshots: X-point formation (XPF), Start of Heating(SOH), the Start of Flattop (SOF), End of Flattop (EOF), End Of Cooling(EOC) and End of Currents in the PF coils (EOC).	13
Figure 3.4	Poloidal cross-section of the JT-60SA plasma at the Start of the Flat Top (SOF) for reference Scenario 2. At SOF, the nominal plasma current is 5.5 MA, while the nominal values for poloidal beta β_p and internal inductance l_i are 0.53 and 0.85, respectively.	14
Figure 3.5	Poloidal cross-section of the JT-60SA plasma at the Start of the Flat Top (SOF) for reference Scenario 2. At SOF, the nominal plasma current is 5.5 MA, while the nominal values for poloidal beta β_p and internal inductance l_i are 0.53 and 0.85, respectively. In this figure the 85 gaps used to assess the plasma shape controller performance are shown.	15
Figure 3.6	SOF equilibrium reconstructed from CREATE-NL and the CCS code along with the magnetic field and flux sensors locations	17
Figure 3.7	JT-60SA	18
Figure 3.8	JT-60SA	19
Figure 3.9		19
Figure 3.10		19
Figure 3.11		20

List of Figures

Figure 3.12	Different choices for the set of controlled gaps used for gap controller.	21
Figure 3.13	Comparison of the shape controller performance in the presence of Disturbance #3 (minor disruption). The two cases of 8 and 20 gaps are considered.	21
Figure 5.1	ISTTOK MARTe overall control position scheme	26
Figure 5.2	Fig. 26	
Figure 5.3	Fig. 27	
Figure 5.4	Pole-Zero maps in closed loop for the model when $I_p \approx 4kA$. Superposition of poles and zeros can be seen in the four transfer functions.	27
Figure A.1	Plasma centroid position Shot# 48563 Shot# 48561	42
Figure A.2	lalala Shot# 48563 Shot# 48561	42
Figure A.3	Plasma centroid position Shot# 48556 Shot# 48552	43
Figure A.4	lalala Shot# 48556 Shot# 48552	43
Figure A.5	Plasma centroid position Shot# 48551 Shot# 48554	44
Figure A.6	lalala Shot# 48551 Shot# 48554	44
Figure A.7	Plasma centroid position Shot# 48515 Shot# 48541	45
Figure A.8	lalala Shot# 48515 Shot# 48541	45
Figure A.9	Plasma centroid position Shot# 48544 Shot# 48542	46
Figure A.10	lalala Shot# 48544 Shot# 48542	46
Figure A.11	Plasma centroid position Shot# 48546 Shot# 48548	47
Figure A.12	lalala Shot# 48546 Shot# 48548	47
Figure A.13	Plasma centroid position Shot# 48340 Shot# 48338	48
Figure A.14	lalala Shot# 48340 Shot# 48338	48
Figure A.15	Plasma centroid position Shot# 48343 Shot# 48342	49
Figure A.16	lalala Shot# 48343 Shot# 48342	49
Figure A.17	Plasma centroid position Shot# 48346 Shot# 48345	50
Figure A.18	lalala Shot# 48346 Shot# 48345	50
Figure A.19	Plasma centroid position Shot# 48349 Shot# 48348	51
Figure A.20	lalala Shot# 48349 Shot# 48348	51
Figure A.21	Plasma centroid position Shot# 48352 Shot# 48354	52
Figure A.22	lalala Shot# 48352 Shot# 48354	52
Figure A.23	Plasma centroid position Shot# 48351 Shot# 48350	53
Figure A.24	lalala Shot# 48351 Shot# 48350	53

LIST OF TABLES

Table 3.1	X-point position steady state error for a given JT60-SA scenario in the presence of a minor disruption. The XSC and QST controller were used in different simulations for the shape control along with two reconstruction methods for the LCFS.	20
Table 3.2		20
Table 5.1	Centroid position RMSE comparison between PID and MIMO-LQR controlled discharges for different set points and plasma current scenarios.	32

LIST OF ABBREVIATIONS

@TODO: Review variable lists as writing the thesis

- AC - Alternating Current
- ADC - Analog to Digital Converter
- ATCA - Advanced Telecommunications Computing Architecture
- CREATE - Consorzio di Ricerca per l'Energia, l'Automazione e le Tecnologie dell'Elettromagnetismo
- DAC - Digital to Analog Converter
- EO - Electronic Offset
- GAM - Generic Application Module
- IST - Instituto Superior Técnico
- LQR - Linear Quadratic Regulator
- MARTe - Multi-threaded Application Real-Time executor
- MIMO - Multiple-Input Multiple-Output
- PCS - Plasma Control System
- PF - Poloidal Field
- PID - Proportional - Integrative - Derivative
- RFM - Reflective Memory
- SCD - Système de Contrôle Distribué
- XSC - eXtreme Shape Controller
- WO - Wiring Offset

LIST OF VARIABLES

@TODO: Review variable lists as writing the thesis

VARIABLES:

- B_p - Poloidal magnetic field

- I_p - Plasma current
- μ_0 - Vacuum permeability

1

INTRODUCTION

1.1 TOKAMAK PLASMA CONTROL

1.2 BEHIND THE PLASMA CURRENT

1.3 THESIS OUTLINE

2

PLASMA CONTROL SYSTEMS

2.1 OVERVIEW OF CONTROL SYSTEMS

The control of plasma position, shape and current among other parameters is one of the crucial engineering problems for present and future magnetic confinement devices. The Plasma Control Systems (PCS) lead with the overall control of fusion devices being responsible also for the plasma configuration and scenarios algorithms [1, Chapter 8]. Currently different PCS's are use in the tokamaks around the world. In this chapter the "DIII-D-like" PCS, the Système de Contrôle Distribué (SCD) and the Multi-threaded Application Real-Time executor (MARTe) will be approach, this last one being of special interest due to its extensive utilization in this work.

2.1.1 *DIII-D Plasma Control System*

The DIII-D-like PCS is use in various fusion research facilities such as EAST(China), K-STAR (South Korea) and MAST (UK). Early documentation regarding the PCS in DIII-D¹ reefers to digitalization of analog signals transmitted to a high speed processor executing a shape control algorithm and then writing the result to a digital to analog converter for driving the controlled systems . The real-time computer used allowed to performed operations with vectors and matrices required for the plasma shape control algorithm [2]. Figure 2.1 shows the block diagram of the DIII-D PCS 30 years ago.

In recent years the DIII-D PCS had extensive software and hardware upgrades. The PCS actual software consists of an infrastructure library core which provides all the routines that are necessary for implementing a basic and generic control system. The current PCS hardware configuration uses a collection of Intel Linux based multi-processor computers running in parallel to perform the real-time analysis and feedback control [3]. New digitizers have been added to the real-time network to increase the number of signals acquired an to control hardware on real-time, several real-time control algorithms were added and real-time data was added to external entities such as web server. [4]. In

¹ DIII-D is a D-shape tokamak operated by General Atomics in San Diego, California.

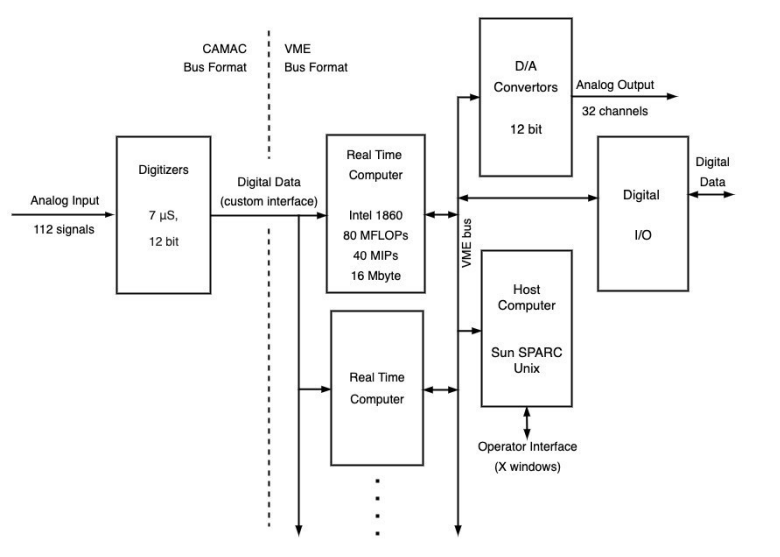


Figure 2.1.: DIII-D digital PCS in 1991 [2].

the current version of the PCS, a Myricom² network has been replaced with a 40 Gb/sec InfiniBand³ network based on the Mellanox Connect-X 3⁴ hardware set. Figure 2.2 shows the currently overall networking diagram of DIII-D PCS .

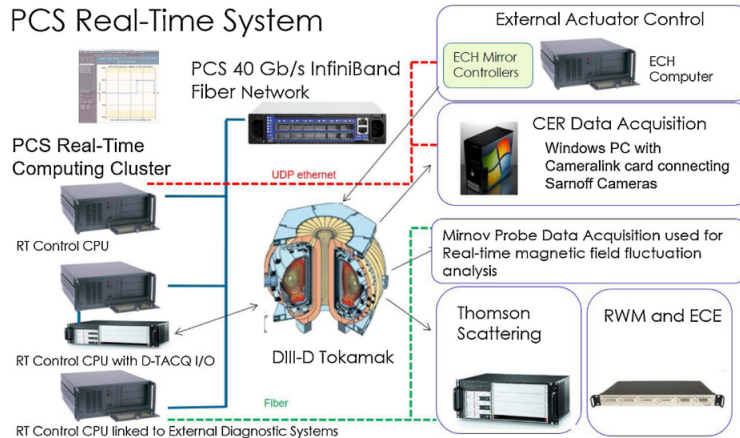


Figure 2.2.: Actual DIII-D PCS real-time systems [4].

² Myricom networks also called Myrnet are high speed networking systems used to interconnect machines to form computer clusters.

³ Is a network architecture from Mellanox designed to support I/O connectivity and reliability, availability, and serviceability Internet requirements [5].

⁴ The Connect-X from the Mellanox company are Ethernet network interface cards with PCI Express.

2.1.2 Système de Contrôle Distribué

The TCV⁵ distributed control system uses a modular network of real time PC nodes liken by a real time network to provide feedback control over all of the actuator systems. Each node consists of a Linux PC either embedded on a Compact-PCI module or as a desktop computer with Intel CPU. A fiber optic ring network links the reflective memory (RFM) network cards in each node [6]. The design of the diagnostic signal processing and control algorithms is performed in Matlab-Simulink software. During the real-time execution C/C++ code is generated from the Simulink and compiled into a Linux shared library and distributed to target nodes providing the input/output interface to the control algorithm code [7]. Figure 2.3 depicts the TCV SCD layout with the connectivity to diagnostics and actuators.

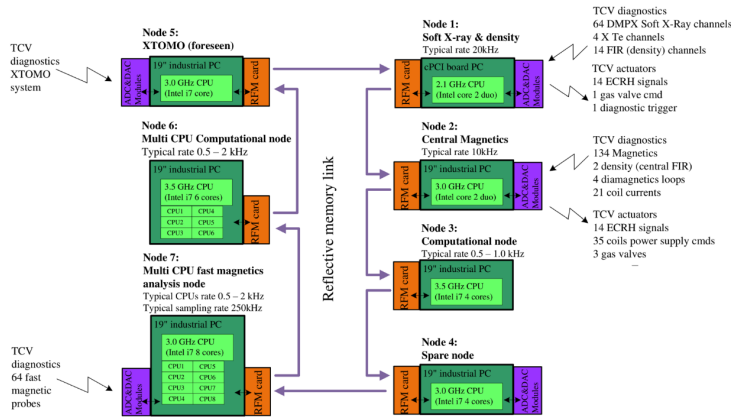


Figure 2.3.: TCV SCD. Real-time network nodes connection. The nodes configurations are shown together with the typical diagnostic and actuator systems to which they are connected [7].

2.2 MARTE FRAMEWORK

Regardless the nature of a real-time system the design of it is usually related to the specific requirements it has, commonly this implies to have customized hardware and software which causes a lack in modularity and portability. When systems become bigger is convenient to provide a common library containing shareable functionalities and which also allows for modular implementations. In order to deal with this the MARTE framework was designed about a decade ago. MARTE was developed in order to standardize general real-time control systems for the execution of control algorithms and is based on a multiplatform C++ library [8]. Previous implementations for a software framework similar to MARTE were developed some years before for the JET tokamak. JETRT was a software framework used to develop real-time control and data acquisition systems which laid the foundation for current MARTE framework [9]. MARTE is currently used in several tokamaks such as JET, FTU, COMPASS and ISTTOK.

⁵ The Tokamak à configuration variable (TCV) is a medium size tokamak localized in Laussane, Switzerland. It is characterized by a highly elongated, rectangular vacuum vessel.

2.2.1 MARTe architecture

The unitary MARTe component is the Generic Application Module (GAM), each of the C++ programmed GAMs usually performs an specific task of the control system, the collection of interconnecting GAMs builds MARTe [10]. The GAMs have an entry point to receive data driven configuration and a set of input and output channels to interface with other GAMs. The Dynamic Data Buffer (DDB) is a generic memory data bus where each GAM receives and produce data using DDB named channels. Usually each GAM is associated with a special function of the system like processing data of an specific diagnostic or perform some control algorithm. MARTe hardware data interface and synchronization for inputs and outputs is performed using a special GAM called IOGAM .

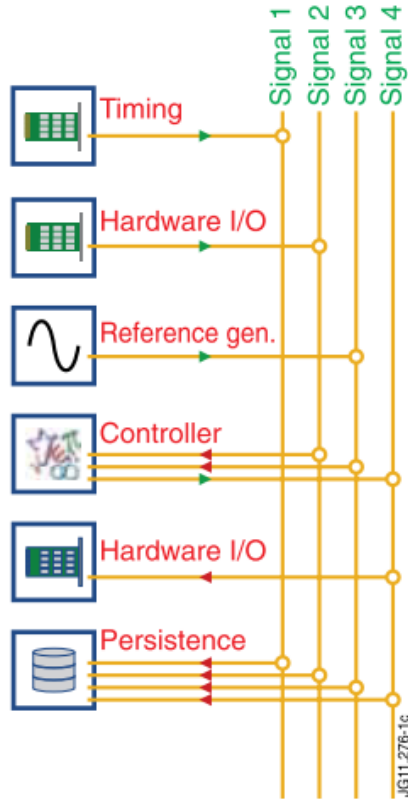


Figure 2.4.: Example of a set of GAMs connected to the DDB. Timing and hardware GAMs provide the I/O interface to the exterior, whereas a generic waveform GAM inputs the reference for a PID controller. Finally, the output is sent to a DAC and the data is stored for analysis by a collection GAM. It should be noticed that the reference generation and the controller GAM are not aware of the changes in the data providers and data consumers. [11]

2.2.2 Hardware containers

The MARTe hardware containers

2.2.3 MARTe 2.0

Software Quality Assurance (QA) processes are being applied to the development of a new version of the MARTe framework also called MARTe 2.0.

[12]

2.3 EQUILIBRIUM AND CONTROL ALGORITHMS

The RAPTOR (RApid Plasma Transport simulatOR) code is a model-based control-oriented code that predicts tokamak plasma profile evolution on real-time. [13]

2.3.1 *State-Space models*

2.3.2 *PID control*

Proportional-Integral-Derivative (PID) control

2.3.3 *Multiple-Input Multiple-Output control*

Multiple-Input Multiple-Output (MIMO)

JT60-SA CONTROL DESIGN

3.1 MACHINE DESCRIPTION

JT60-SA is an under-construction superconductive tokamak located at one of the facilities from the National Institutes for Quantum and Radiological Science and Technology (QST) at Naka, Japan whose principal purpose is the contribution to early realization of fusion energy by supporting the exploitation and resolving key physics for ITER reactor. Figure 3.1 shows the overall general configuration and the most remarkable elements of the machine. The JT-60SA vacuum chamber will have a major radius of 2.96 m and a minor radius of 1.18 m with an overall plasma volume of 132 m^3 [14].

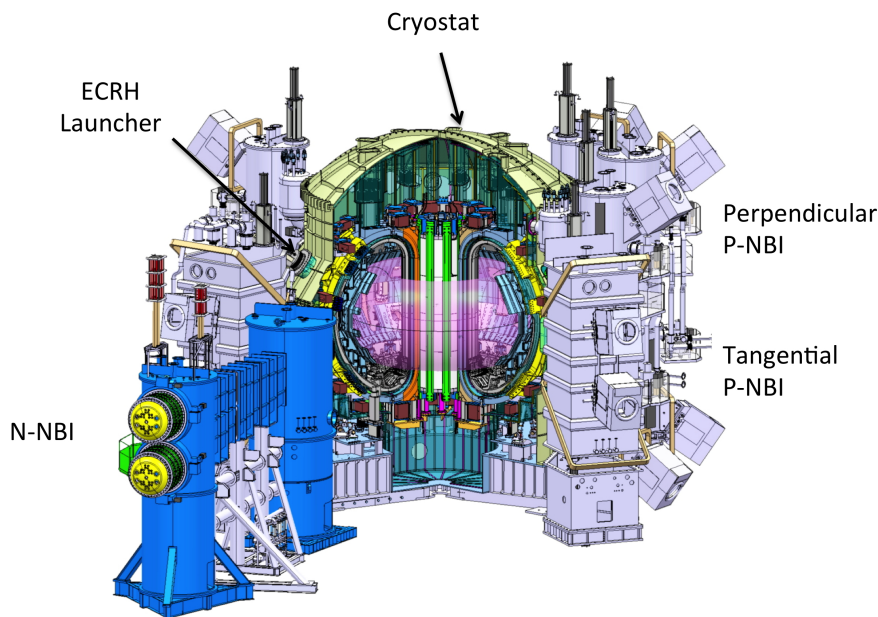


Figure 3.1.: JT60-SA tokamak configuration and its main elements [15].

The Poloidal Field (PF) coils shown in JT60-SA cross-section from figure 3.2 consist of two sets of superconductive coils: the Equilibrium Field Coils (EF1–6) and the Central Solenoid (consisting of four independent coils, named CS1–4). Furthermore, two in-vessel Fast Plasma Position copper Coils

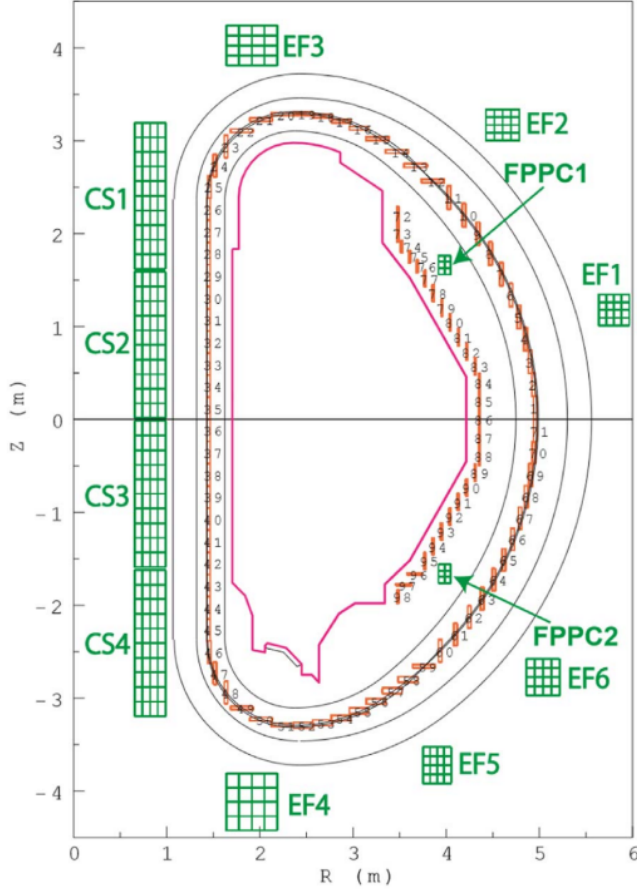


Figure 3.2.: JT-60SA poloidal cross-section and layout of the Poloidal Field coils system [16].

(FPPC1–2) will also be installed [16].The total of 12 PF coils have independent power sources value for the control of the plasma current, position and shape.

JT-60SA shall be capable of investigating different design scenarios. As referred in [17] it exists a set of 6 reference scenarios, additional ones, including some with a shorter repetition rate will be defined in future. For the control study in this section all simulations will be built based on the Scenario 2 characteristics. In particular, Scenario 2 refers to a 5.5 MA inductive lower single null discharge.The Scenario 2 its divided in 5 time snapshots with different equilibrium each one starting at $t=-40$ s until $t=177.96$ s. The different Last Closed Flux Surfaces (LCFS) for each time window are shown in figure 3.3, the time sequence starts at the X-point formation (XPF) followed by the Start of Heating(SOH), the Start of Flattop (SOF), End of Flattop (EOF), End Of Cooling(EOC) and finishing with the End of Currents in the PF coils (EOC). In this section reconstruction methods and control algorithms will be based on the *Start of Flattop* (SOF) equilibrium shown in figure 3.4. The nominal values for the plasma current, the poloidal beta and the internal inductance for Scenario 2 at SOF are $I_{peq} = 5.5$ MA, $\beta_{peq} = 0.53$, and $l_{ieq} = 0.85$.

This chapter will address two different approaches for the LCFS reconstruction along with different plasma current, shape and position controllers on JT60-SA in order to achieve and maintain the desired

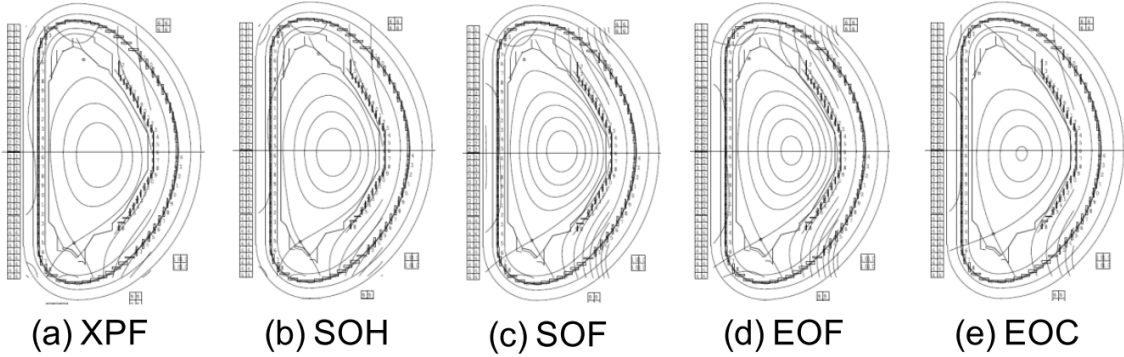


Figure 3.3.: LCFS Equilibria corresponding to the different Scenario 2 snapshots: X-point formation (XPF), Start of Heating(SOH), the Start of flattop (SOF), End of flattop (EOF), and End Of Cooling(EOC).

operational scenario given the plasma equilibrium in the SOF while the performance of the controllers is compared .

3.2 CREATE MAGNETIC RECONSTRUCTION TOOLS

CREATE-NL (Consorzio di Ricerca per l' Energia, l' Automazione e le Tecnologie dell' Elettromagnetismo) is a finite elements method (FEM¹) solver implemented on MATLAB. It deals with the free boundary dynamic plasma equilibrium problem i.e. the MHD (Magneto Hydro Dynamics) time evolution of 2D axisymmetric plasmas in tokamaks, including eddy currents in the passive structures, and feedback control laws for current, position and shape control [18].

Using the CREATE codes [18,19] it is possible to retrieve a linearized state-space model that describes the plasma magnetic behavior around that equilibrium².It shoudl be noted that CREATE-NL equilibrium solver has been validated on several tokamaks such as JET and EAST.

A JT60-SA CREATE-NL electromagnetic linear model around the equilibrium from the Scenario 2-SOF for the plasma-circuit response has been used for designing the controller presented in next section.

3.3 CONTROLLER DESIGN

The JET (Joint European Torus) tokamak was the first machine where around 2005 a new model based plasma current and shape controller was set up and tested with the existing active circuits and control hardware. The novelty controller was the eXtreme Shape Controller (XSC) and its aim was to

¹ It is well known that many physical and engineering systems are expressed in terms of partial differential equations which cannot be solved via analytical methods. One of the most recurrent techniques is numerical discretization to approximate the solution of the partial differential equations, the FEM is commonly used to solve these approximations in two or three space variables, in this particular case for a numerical solution of the well-known Grad-Shafranov equation.

² Reference [16, Sec. 3] can be consulted for more details about the use of the CREATE equilibrium codes to retrieve plasma linearized models.

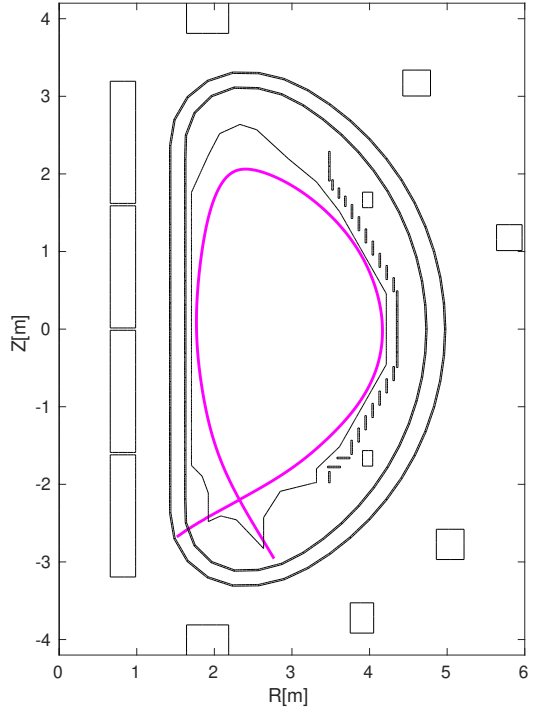


Figure 3.4.: Poloidal cross-section of the JT-60SA plasma at the Start of the Flat Top (SOF) for reference Scenario 2. At SOF, the nominal plasma current is 5.5 MA, while the nominal values for poloidal beta β_p and internal inductance l_i are 0.53 and 0.85, respectively.

improve the performance of the back then present controller to allow the control of extremely shaped plasmas with higher values of elongation and triangularity [20]. More recently this control approach was utilized at TCV [21]. At JET, the XSC recently enabled the control of high triangularity shapes with both strike points in the divertor corner, which has a large impact in the H-mode confinement in the case of ITER-like wall at JET [22].

Usually the controlled shape geometrical descriptors are the distances between the plasma boundary and the vessel at some specific points. These plasma-wall distances are called gaps [23]. The gaps are segments that can be used to describe the shape of the plasma boundary. Being g_i the abscissa along the i -th control segment, we assume that $g_i = 0$ at the first wall. *Gap-based* plasma shape control is achieved by controlling to zero the difference $g_{i,ref} - g_i$ on a sufficiently large number of gaps, being $g_{i,ref}$ the value of the abscissa on the i -th control segment for the reference shape. Figure 3.5 shows a poloidal cross-section of JT-60SA together with a set of 85 gaps used for the assessment of the plasma shape control.

The XSC algorithm can be used either to implement a gap-based control strategy, or an isoflux one, as it has been proposed in [16]. The isoflux strategy consists in controlling the X-point position along with a set of flux differences between the flux at some selected control points along the desired plasma boundary and the X-point flux.

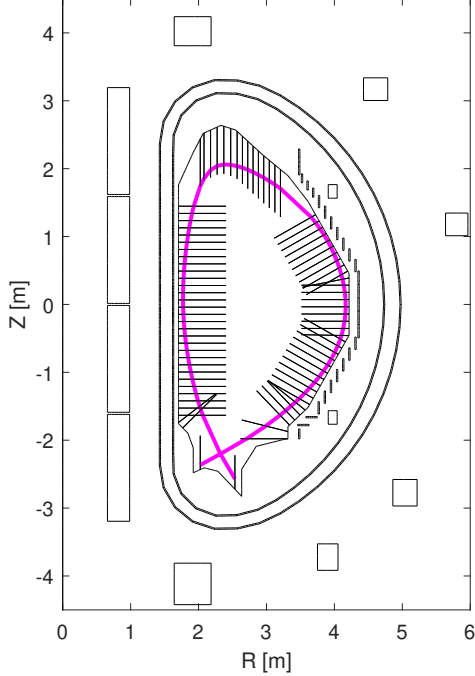


Figure 3.5.: Poloidal cross-section of the JT-60SA plasma at the Start of the Flat Top (SOF) for reference Scenario 2. At SOF, the nominal plasma current is 5.5 MA, while the nominal values for poloidal beta β_p and internal inductance l_i are 0.53 and 0.85, respectively. In this figure the 85 gaps used to assess the plasma shape controller performance are shown.

The peculiarity of the XSC approach is that it permits to control a number of plasma shape descriptors that is greater than the number of available actuators, i.e. of PF Circuits, this is basically tackled by using a singular value decomposition (SVD) to identify the principal directions of the algebraic mapping between coil currents and geometrical descriptors [20]. The XSC control relies on the PFC decoupling controller (more details can be found in [16, Section 4.4]), since it is assumed that each PFC can be treated as an independent single-input-single-output channel whose dynamic response is modeled in the Laplace domain by

$$I_{PF_i}(s) = \frac{I_{PF_{ref,i}}(s)}{1 + s\tau_{PF}},$$

where I_{PF_i} and $I_{PF_{ref,i}}$ are the Laplace transform of the measured and reference current in the i -th PFC, respectively, and where it is assumed that all the PFC exhibit the same bandwidth (i.e., they have the same time constant τ_{PF}).

Denoting by $\delta Y(s)$ the Laplace transform of the variations of the n_G gaps to be controlled, it is possible to exploit the CREATE electromagnetic linear model [16] that links the variation of the PFC reference currents $\delta I_{PF_{ref}}$ to $\delta Y(s)$, i.e.

$$\delta Y(s) = C \frac{\delta I_{PF_{ref}}(s)}{1 + s\tau_{PF}},$$

which, at steady-state, implies $\delta Y(s) = C\delta I_{PF_{ref}}(s)$.

If the number of controlled plasma shape descriptors n_G is such that $n_G > n_{PF}$, the XSC computes the additional current references as

$$\delta I_{PF_{ref}} = C^\dagger \delta Y. \quad (3.1)$$

where the matrix C^\dagger denotes the pseudo-inverse of C^3 that can be computed via the singular value decomposition (SVD). As a result, the XSC algorithm minimizes the following steady-state performance index

$$J_{XSC} = \lim_{t \rightarrow +\infty} (\delta Y_{ref} - \delta Y(t))^T (\delta Y_{ref} - \delta Y(t)), \quad (3.2)$$

where δY_{ref} are constant references for the geometrical descriptors. When the SVD of the C matrix is used to minimize (3.2), it may happen that some singular values (depending on the plasma configuration) are one order of magnitude smaller than the others. This fact implies that minimizing the performance index (3.2) retaining all the singular values results in a large control effort at the steady-state, that is a large request on some PFC currents which have only a minor effect on the plasma shape. In order to minimize also the control effort, the additional references (3.1) are generated by using only the $\bar{n} < n_{PF}$ linear combinations of PF currents which are related to the largest singular values of the C matrix. This is achieved by using only the \bar{n} singular values when computing the pseudo-inverse C^\dagger .

Moreover, the PFC current variations given by (3.1) are summed to the scenario currents and sent to the PFC decoupling controller as references to be tracked. It is worth to remark here that the dynamnic behaviour of the XSC is improved by adding a set of proportional-integral-derivative (PID) controllers on each PFC channel (see [24] for a complete description of the XSC control scheme).

For the development of this work both approaches of the XSC strategy were studied and simulated for a different number of control points: isoflux and gap-based controllers. In addition, a second controller developed by the QST team was implemented in the simulations, the features of this controller will be detailed in the next section.

3.4 QST RECONSTRUCTION AND CONTROL IMPLEMENTATION

Along with the CREATE tools presented above for the reconstruction of the LCFS and the XSC for plasma shape control, a reconstruction code and controller provided by the QST team were tested and compared. This section will briefly describe these two methods and its limitations.

3.4.1 Cauchy Condition Surface reconstruction method

The QST Cauchy Condition Surface (CCS) method for the reconstruction of the magnetic last closed flux surface calculates controlled variables for plasma position and shape control such as the poloidal

³ C is the output matrix from the state-space linearized CREATE model for JT60-SA.

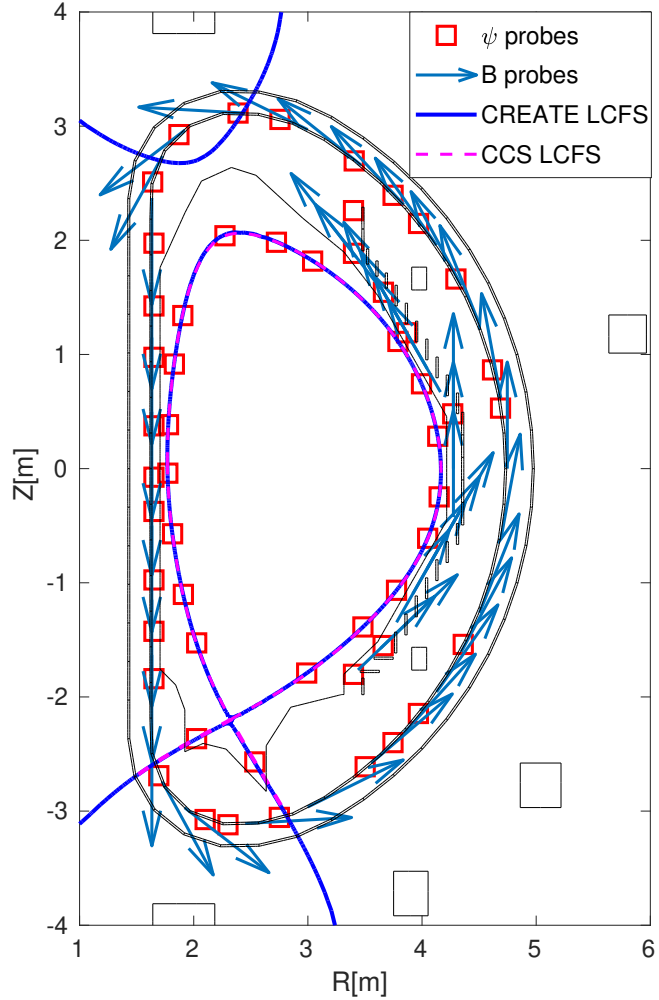


Figure 3.6.: SOF equilibrium reconstructed from CREATE-NL and the CCS code along with the magnetic field and flux sensors locations

magnetic flux at control points on an isoflux scheme [25]. The CCS method allows a selection up to 19 geometrical control points and its input parameters are the current in the PF coils, the measurements in the magnetic field and flux sensors and the plasma current. The output signals from the CCS reconstruction method are the magnetic fluxes at the X-point and the selected control points.

3.4.2 QST magnetic controller (FBC)

The QST magnetic controller FBC uses the PF coils signals to control the plasma current I_p and the FPPC coils signals for plasma position control [26].

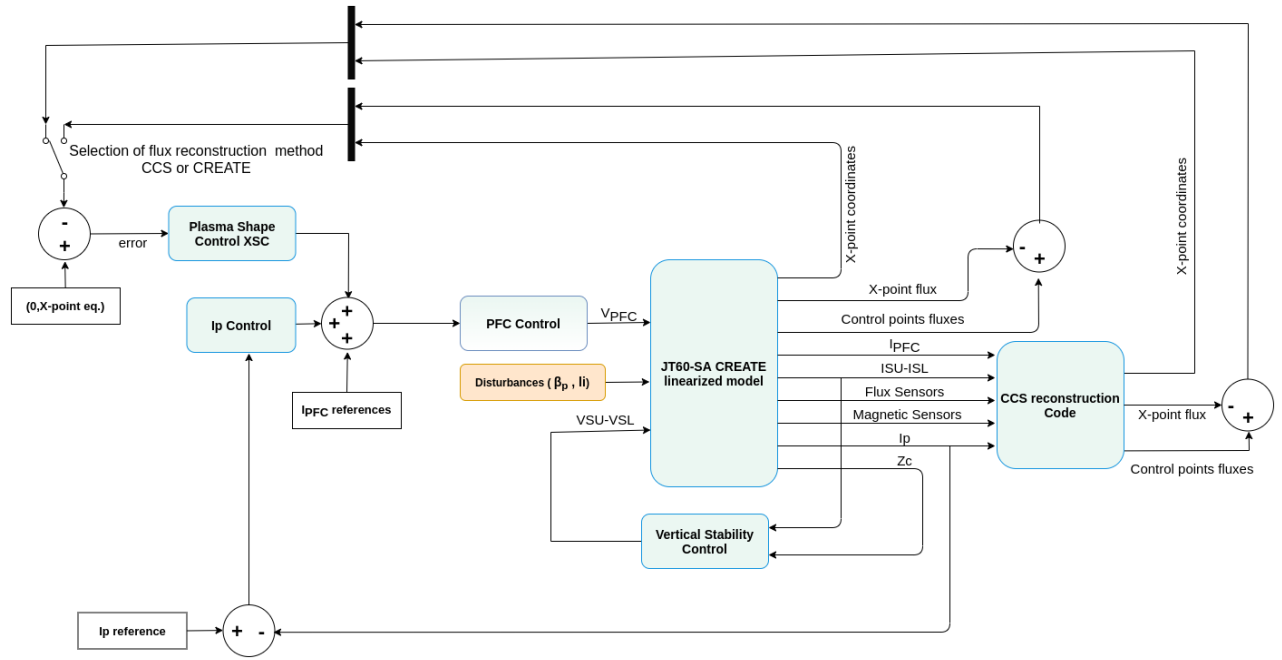


Figure 3.7.: JT-60SA

QST magnetic controller calculates command values of active coil currents/voltages from some information

$$I_{PF_ref}(t + \Delta t) = I_{PF}(t_0) + M_{PF}^\dagger \left[G_{SP} \delta \Psi_s(t) + G_{SI} \int_{t_0}^t \delta \Psi_s(t) dt + G_{XP} \delta \Psi_X(t) + G_{XI} \int_{t_0}^t \delta \Psi_X(t) dt \right] \quad (3.3)$$

$$V_{com} = G_{vt} \left[M_{coil} \frac{(I_{coil_ref} - I_{coil_meas})}{dt} + \frac{M_{plasma_now} \cdot I_{p_now} - M_{plasma_bfr} \cdot I_{p_bfr}}{dt} \right] \quad (3.4)$$

$$I_{FPPC_ref}(t + \Delta t) = I_{FPPC}(t_0) + M_{FPPC}^\dagger \left[G_{FP} \delta \Psi_{SF}(t) + G_{FD} \frac{d}{dt} \delta \Psi_{SF}(t) \right] \quad (3.5)$$

3.5 SIMULATION RESULTS

The simulations for the JT60-SA CREATE-NL model, the XSC, the CCS reconstruction method and the QST controller were programmed on top of MATLAB and SIMULINK blocks. This section will address in detail the outcome of the control simulations

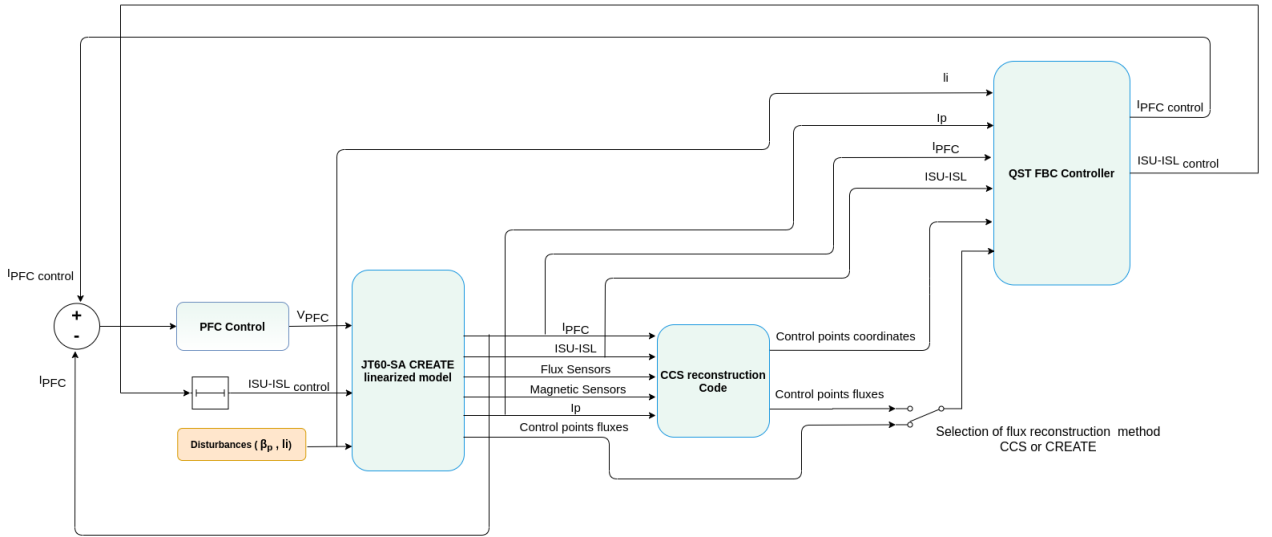


Figure 3.8.: JT-60SA

3.5.1 Disturbances

- **Disturbance #1** refers to the behaviour of β_p and l_i soon after the current flattop is reached, as it was modeled in [?] (in this paper we assume that the flattop is reached at $t \sim 16$ s). As an example, the correspondent time traces are shown in Fig. ??⁴.
- **Disturbance #2** refers to the behaviour of β_p due to the presence of an Edge-Localized Mode (ELM). As described in [17, p. 34], during the flattop an instantaneous drop in β_p of $0.05 \beta_{p_{eq}}$ is followed by an exponential recovery with a time constant of 0.05 s with a frequency 10 Hz. Note that for this disturbance l_i does not change.
- **Disturbance #3** refers to the behaviour of β_p and l_i when a compound ELM⁵ appear during the flattop [17, p. 34]. The time trace of β_p is the same as in the case of Disturbance #2, l_i is described by an instantaneous drop of 0.06 ($l_{i_{eq}} - 0.5$) followed by an exponential recovery with a time constant of 0.05 s with a frequency 10 Hz. The time traces for β_p and l_i are described in Fig. ??.

3.5.2 Gap-based XSC

3.5.3 Isoflux XSC and QST controller

3.5.4 Shape reference change

⁴ The time behaviour of both β_p and l_i have been estimated starting from the spatial profiles for both plasma density and temperature envisaged for Scenario 2.

⁵ A compound ELM is commonly referred as multiple clearly distinguishable crash events causing large energy losses [?].

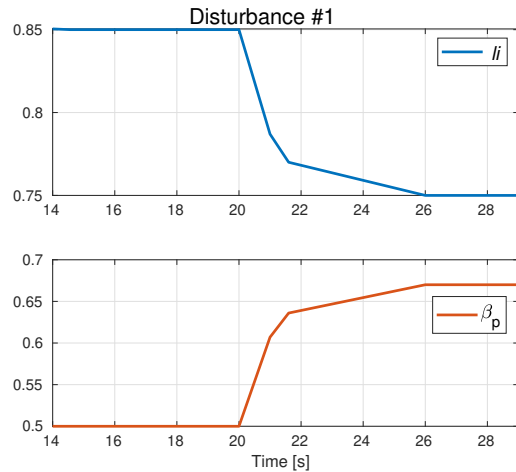


Figure 3.9.

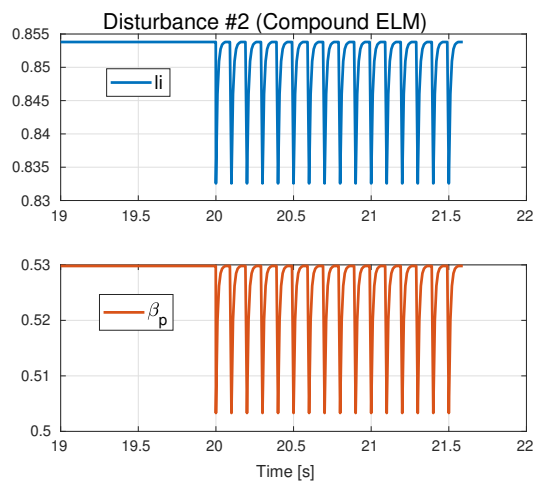


Figure 3.10.

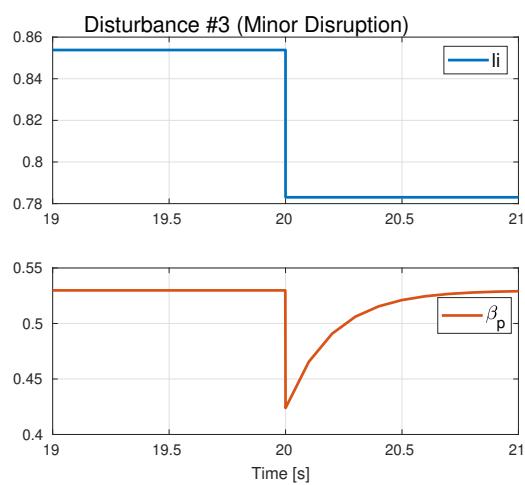
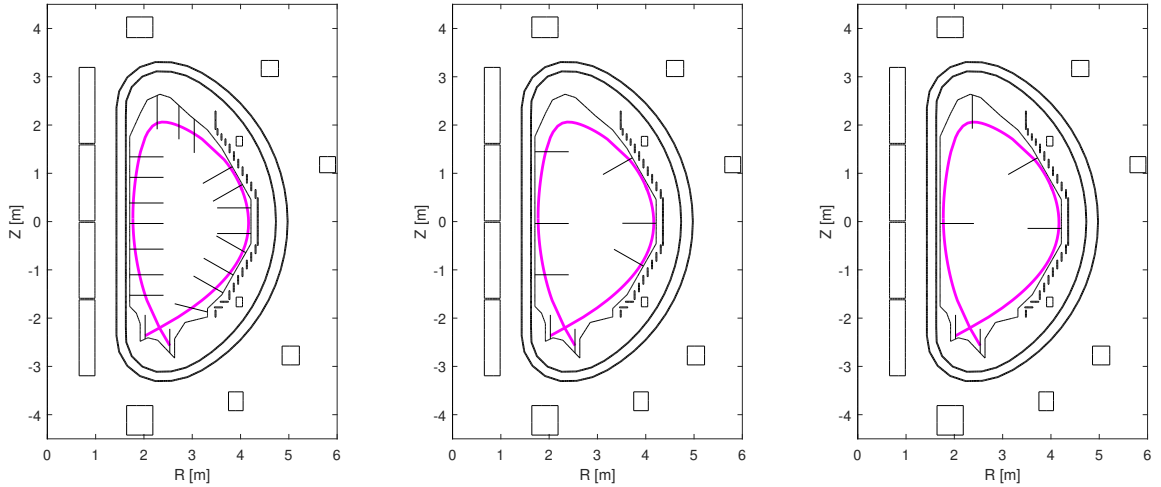


Figure 3.11.



(a) The 20 gaps used to assess the performance of plasma shape controller.
 (b) The 8 control segments by the isoflux controller proposed in [27].
 (c) The 6 control segments used by the isoflux controller proposed in [28].

Figure 3.12.: Different choices for the set of controlled gaps used for gap controller.

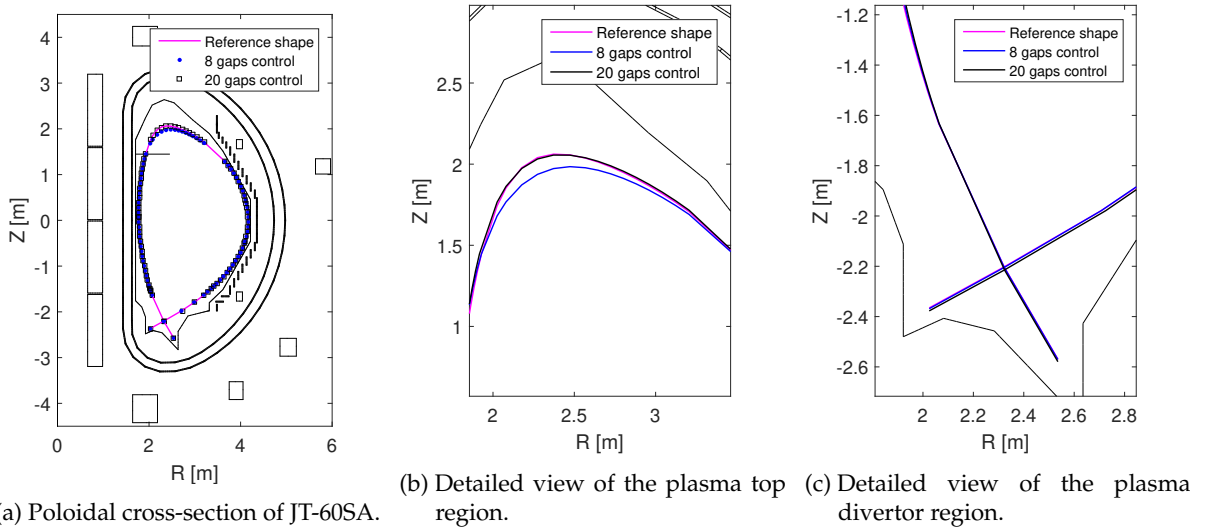


Figure 3.13.: Comparison of the shape controller performance in the presence of Disturbance #3 (minor disruption). The two cases of 8 and 20 gaps are considered.

Disturbance #3 (Minor disruption) steady state X-point error								
Controller	eXtreme Shape Controller				QST Controller			
LCFS reconstruction method	CCS		CREATE		CCS		CREATE	
	Rx mm	Zx mm	Rx mm	Zx mm	Rx mm	Zx mm	Rx mm	Zx mm
6 points	-4.92	20.9	-3.57	28.8	-2.70	-0.105	-2.24	0.369
8 points	17.44	21.56	17.81	29.04	47.08	-46.56	57.61	-41.42
19 points	-5.54	16.78	-4.42	24.41				

Table 3.1.: X-point position steady state error for a given JT60-SA scenario in the presence of a minor disruption. The XSC and QST controller were used in different simulations for the shape control along with two reconstruction methods for the LCFS.

Disturbance #3 (Minor disruption) flux RMSE steady state Wb/2π				
Controller	eXtreme Shape Controller		QST Controller	
LCFS reconstruction method	CCS	CREATE	CCS	CREATE
6 points	0.0121	0.0139	0.0000259	0.0000228
8 points	0.0152	0.0170	0.0000104	0.0000124
19 points	0.0069	0.0088		

Table 3.2.

4

ISTTOK

4.1 MACHINE DESCRIPTION

4.2 DIAGNOSTICS AND ACTUATORS

4.3 ATCA-MIMO-ISOL BOARDS

4.3.1 *Hardware layout*

4.3.2 *Real-time integration software*

4.4 PLASMA CURRENT MAGNETIC FIELD

Retrieving the contribution of the plasma current in tokamaks ...

The methods of correction of the magnetic error fields due to inaccuracies of tokamak manufacturing and assembly are considered. The problems of the plasma position and shape reconstruction based on magnetic field measurements are discussed.

4.5 PLASMA CENTROID POSITION DETERMINATION

5

ISTTOK RESULTS

This chapter describes the latest implementations in ISTTOK MARTe framework followed by the presentation of the obtained results for control of the current centroid position.

5.1 IMPLEMENTATION OF THE GENERAL APPLICATION MODULES

General Application Modules (GAM)

5.1.1 *PID control implementation*

Proportional-Integrative-Derivative

5.1.2 *Data-driven state-space model retrieving*

Early efforts in finding a real-time equilibrium solver for ISTTOK were performed in the last years. Due to the geometrical conditions it was never retrieve a

5.1.3 *Kalman filter implementation*

5.1.4 *Multiple-Input Multiple-Output control implementation*

5.2 PLASMA CURRUENT CENTROID POSITION CONTROL RESULTS

This section addresses the latest results from the real-time implementation of control algorithms in ISTTOK.

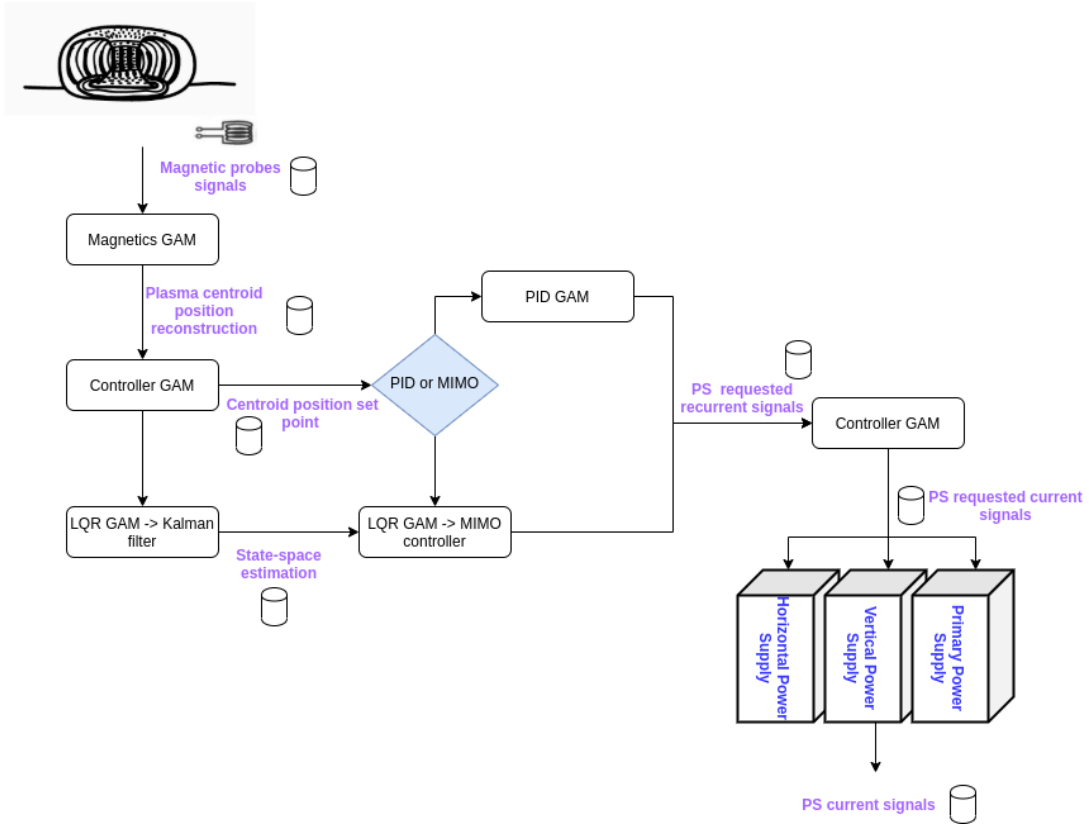


Figure 5.1.: ISTTOK MARTe overall control position scheme

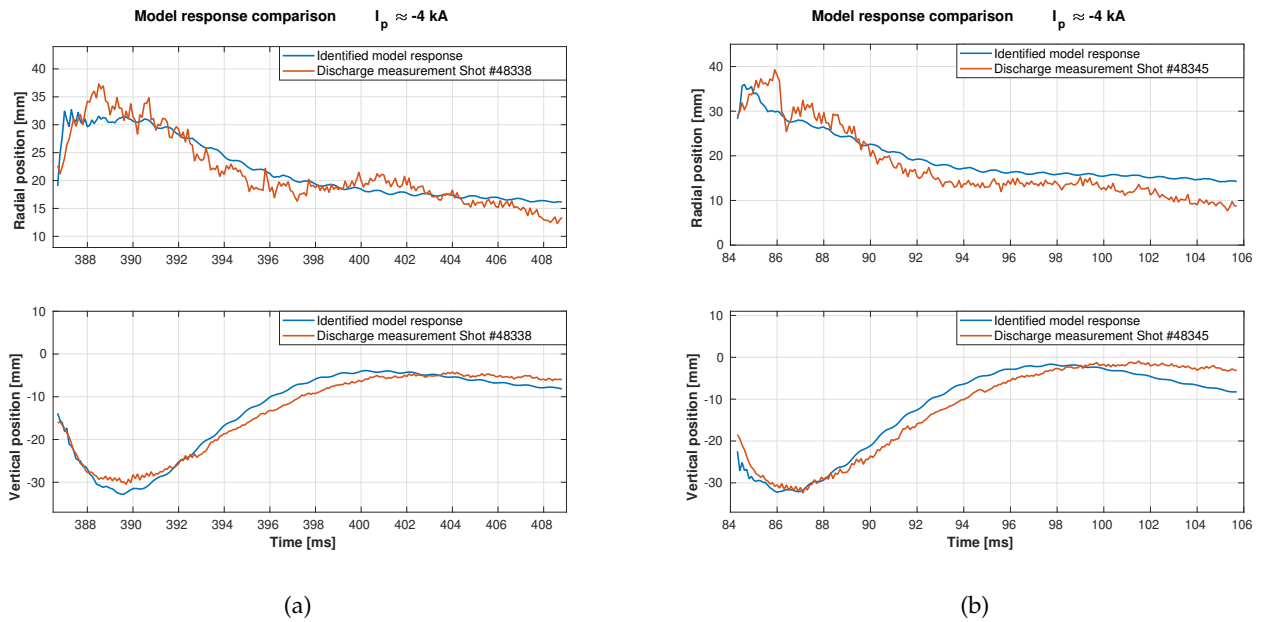


Figure 5.2.: Fig.

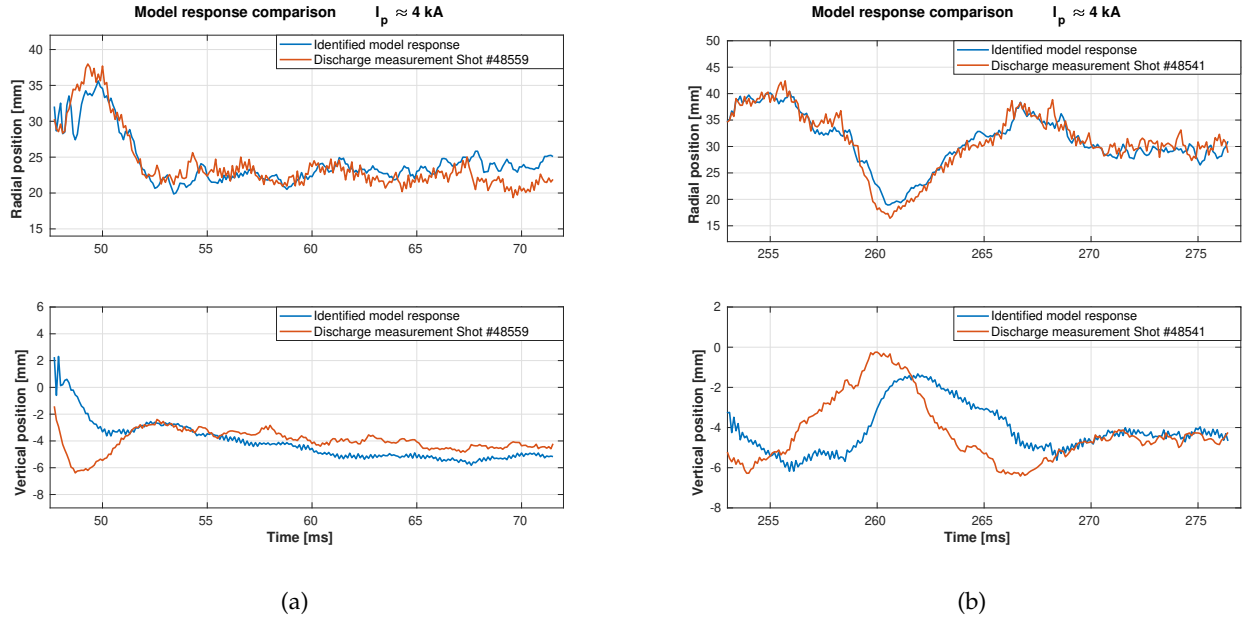
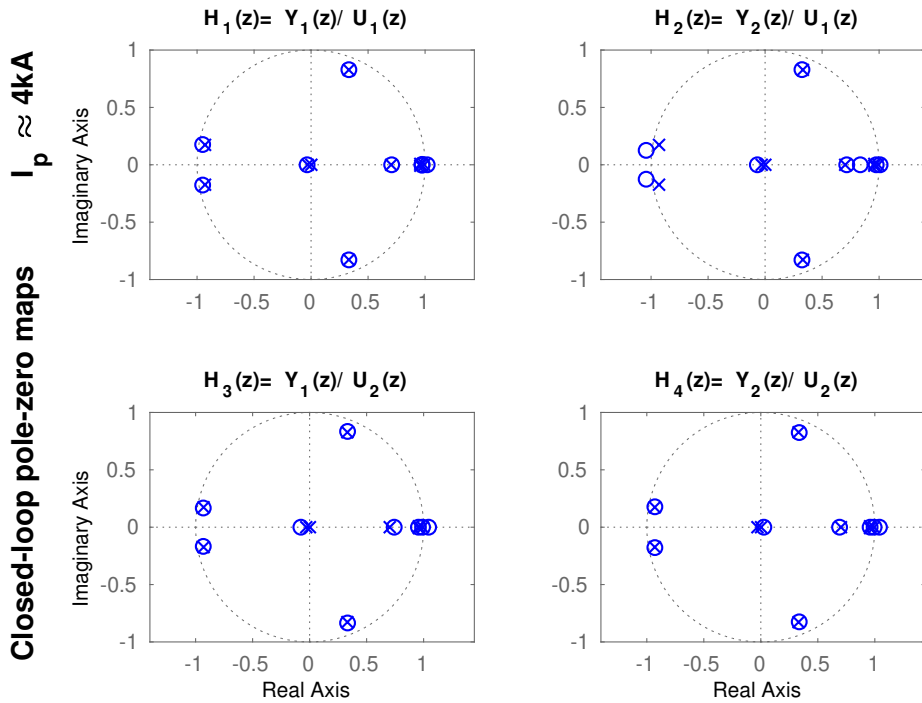
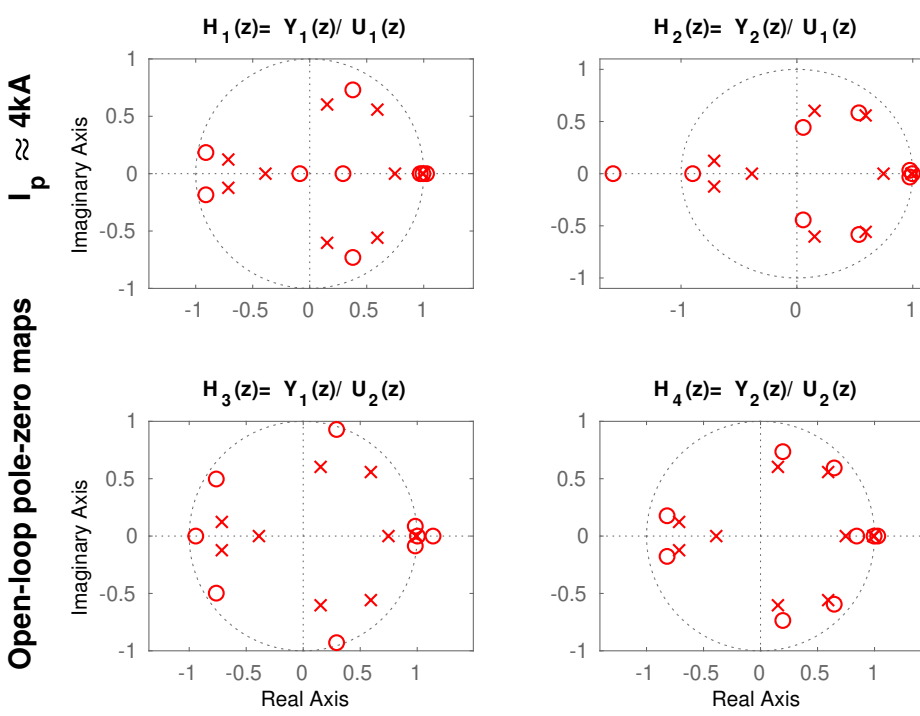
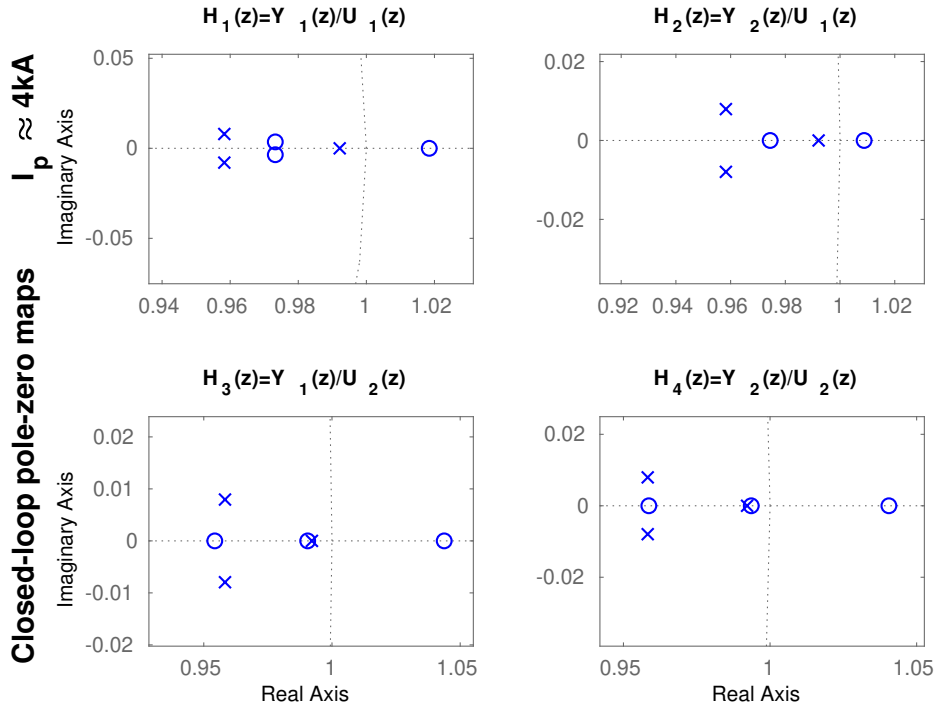
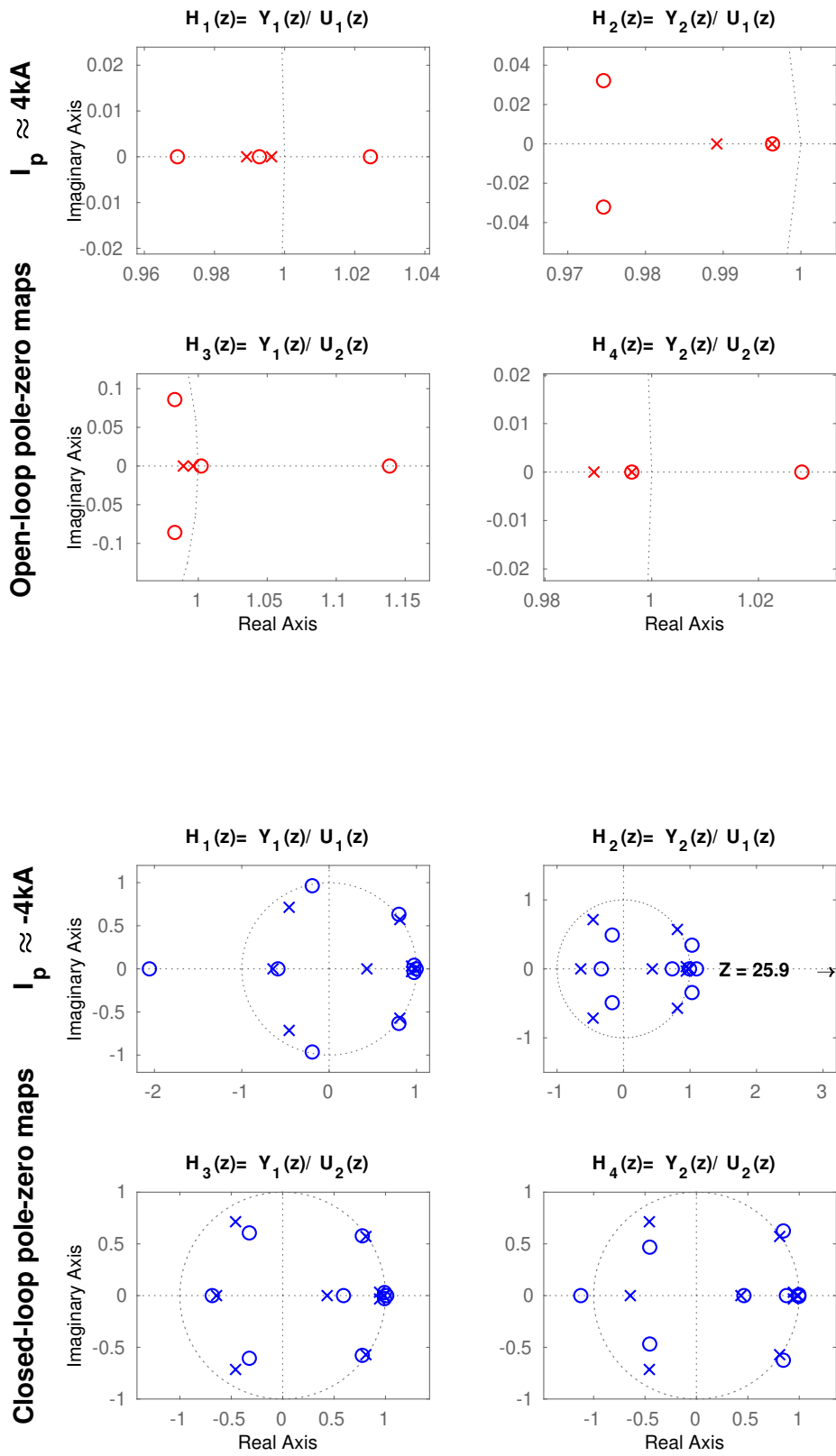
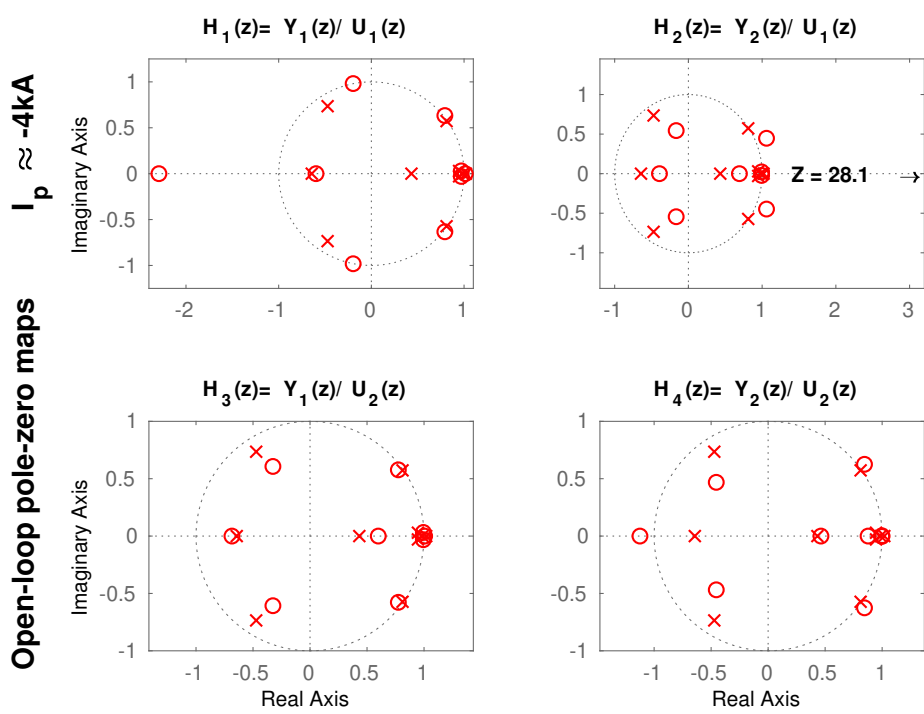
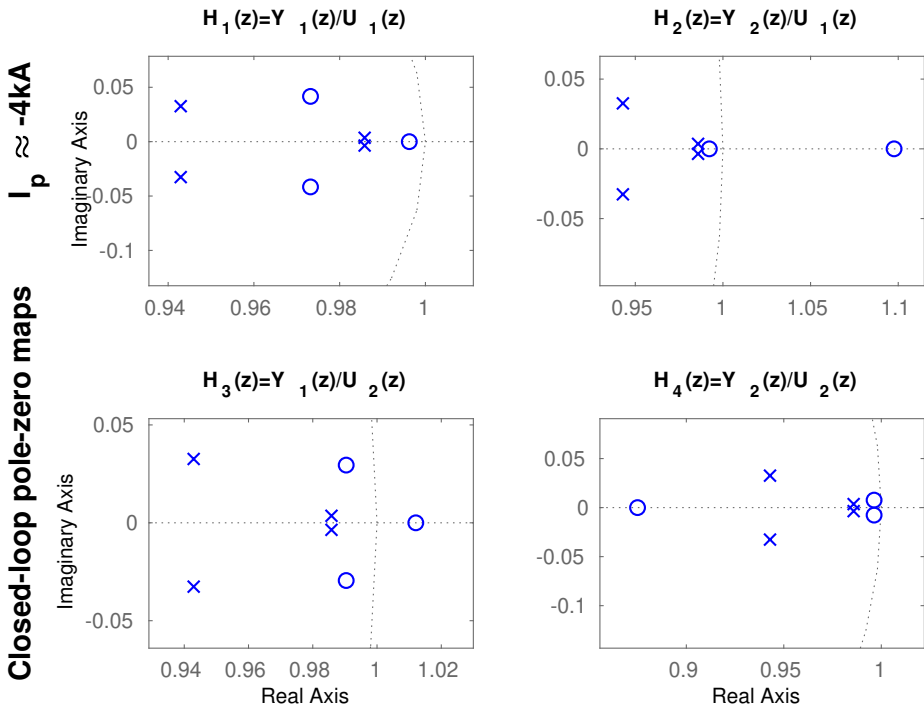


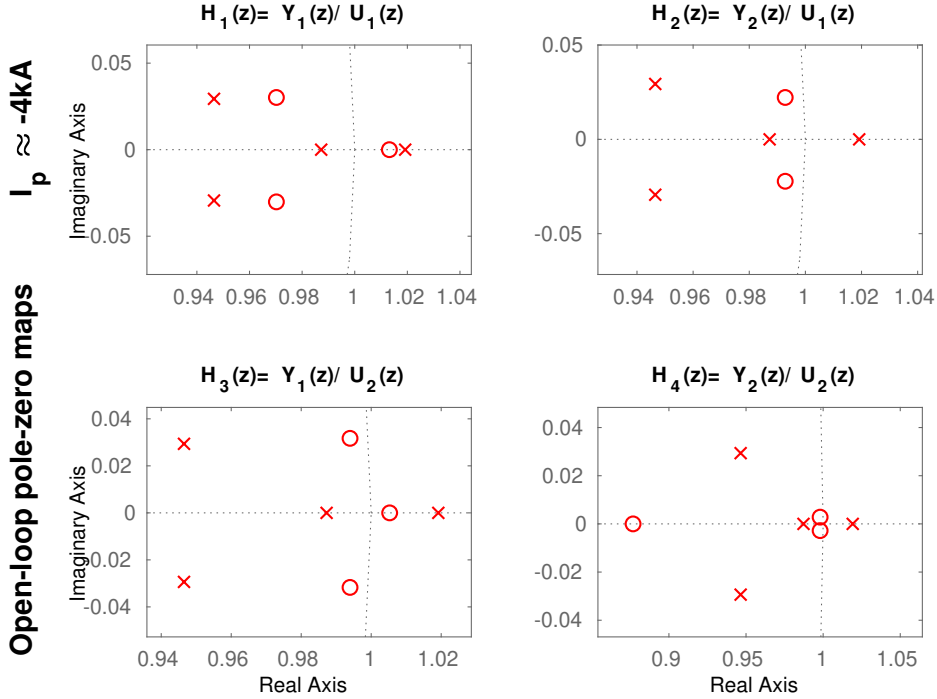
Figure 5.3.: Fig.


 Figure 5.4.: Pole-Zero maps in closed loop for the model when $I_p \approx 4\text{kA}$. Superposition of poles and zeros can be seen in the four transfer functions.









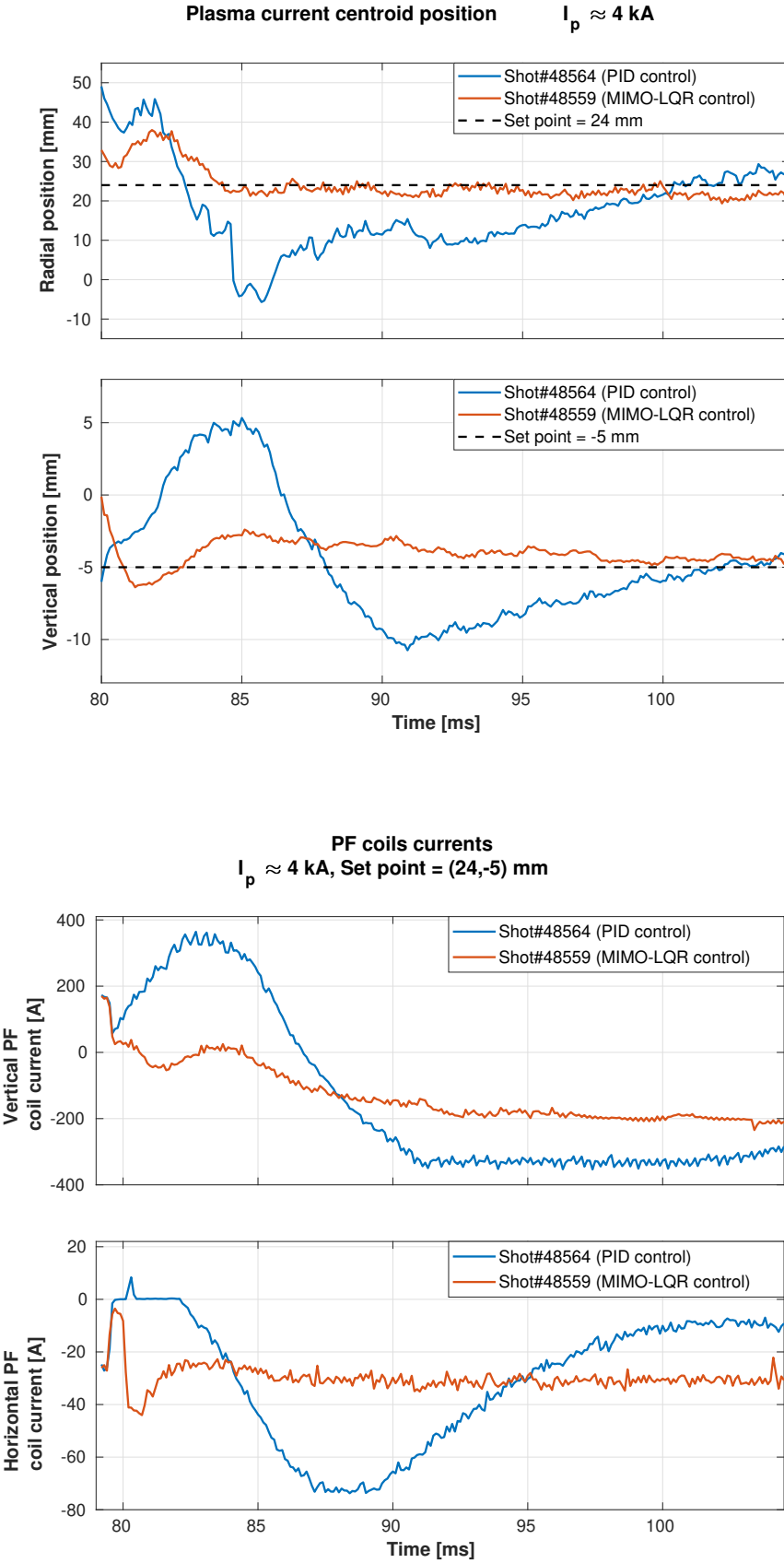
5.2.1 PID control and LQR control results

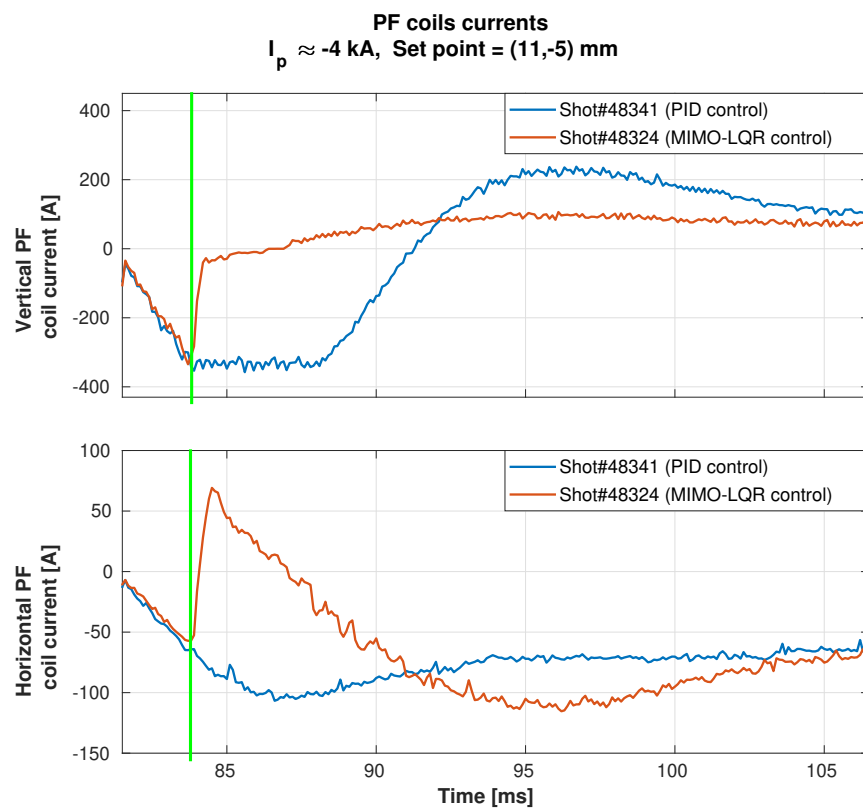
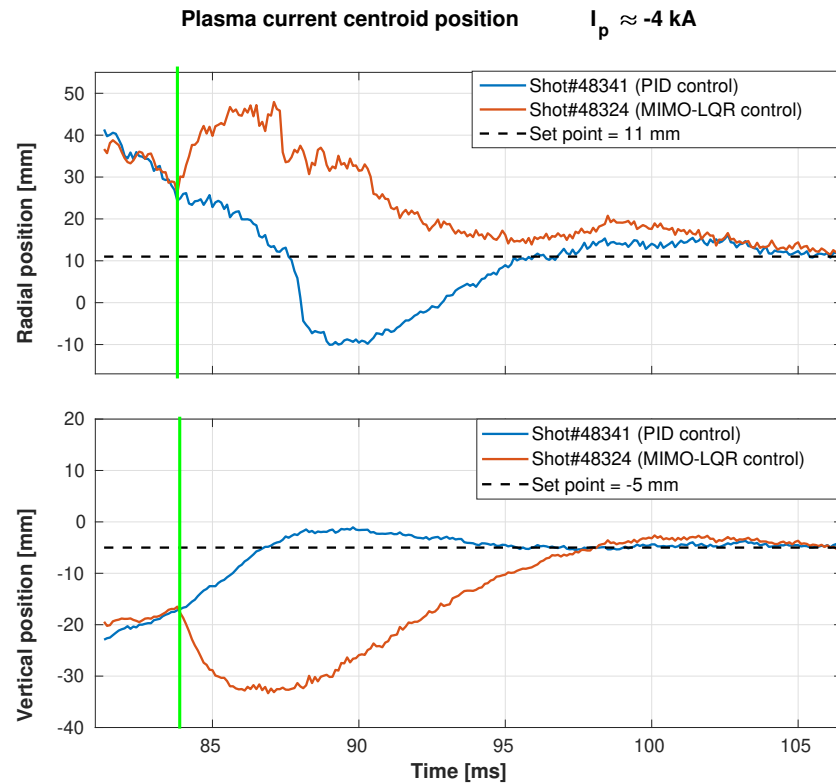
This section addresses obtained the experimental results in ISTTOK's plasma discharges.

Control	Shot #	RMSE (R, z) mm	Set point (R, z) mm	I_p
PID	48564	(13.73, 4.4102)	(24, -5)	$\approx 4kA$
MIMO LQR	48559	(4.2252, 1.4215)	(24, -5)	$\approx 4kA$
PID	48563	(13.6717, 4.1652)	(24, -4)	$\approx 4kA$
MIMO LQR	48561	(8.1047, 3.2752)	(24, -4)	$\approx 4kA$
PID	48556	(12.0315, 3.3217)	(32, -5)	$\approx 4kA$
MIMO LQR	48555	(4.2618, 2.4698)	(32, -5)	$\approx 4kA$
PID	48551	(13.9998, 3.3431)	(27, -5)	$\approx 4kA$
MIMO LQR	48554	(5.9830, 2.0062)	(27, -5)	$\approx 4kA$
PID	48515	(6.0178, 2.6123)	(30, -5)	$\approx 4kA$
MIMO LQR	48541	(5.8372, 1.7664)	(30, -5)	$\approx 4kA$
PID	48544	(4.8745, 2.5167)	(32, -4)	$\approx 4kA$
MIMO LQR	48542	(4.4346, 3.6573)	(32, -4)	$\approx 4kA$
PID	48546	(11.4560, 3.4765)	(27, -7)	$\approx 4kA$
MIMO LQR	48548	(7.6745, 4.1569)	(27, -7)	$\approx 4kA$
PID	48341	(12.0959, 5.7652)	(11, -5)	$\approx -4kA$

MIMO LQR	48324	(15.4768, 14.3436)	(11, -5)	$\approx -4kA$
PID	48340	(11.7701, 5.9599)	(11.2, -5.5)	$\approx -4kA$
MIMO LQR	48338	(11.5260, 12.6226)	(11.2, -5.5)	$\approx -4kA$
PID	48343	(15.7675, 5.7453)	(12, -5)	$\approx -4kA$
MIMO LQR	48342	(14.5168, 14.4329)	(12, -5)	$\approx -4kA$
PID	48346	(12.4228, 6.1541)	(12.2, -5.3)	$\approx -4kA$
MIMO LQR	48345	(9.7513, 13.0338)	(12.2, -5.3)	$\approx -4kA$
PID	48349	(19.3397, 5.5406)	(11.5, -5.6)	$\approx -4kA$
MIMO LQR	48348	(9.1727, 13.1505)	(11.5, -5.6)	$\approx -4kA$
PID	48352	(15.2181, 6.5395)	(10.8, -4.7)	$\approx -4kA$
MIMO LQR	48354	(14.6405, 13.7307)	(10.8, -4.7)	$\approx -4kA$
PID	48351	(13.4078, 5.8769)	(13.2, -5.6)	$\approx -4kA$
MIMO LQR	48350	(13.9320, 14.4940)	(13.2, -5.6)	$\approx -4kA$

Table 5.1.: Centroid position RMSE comparison between PID and MIMO-LQR controlled discharges for different set points and plasma current scenarios.





6

CONCLUSIONS

bla bla bla

BIBLIOGRAPHY

- [1] Andrej A. Kavin Valerij A. Belyakov. *Fundamentals of Magnetic Thermonuclear Reactor Design*. Elsevier, 2018.
- [2] J. R. Ferron, A. Kellman, E. McKee, T. Osborne, P. Petrach, T. S. Taylor, J. Wight, and E. Lazarus. An advanced plasma control system for the dIII-d tokamak. In [*Proceedings*] *The 14th IEEE/NPSS Symposium Fusion Engineering*, pages 761–764 vol.2, Sep. 1991.
- [3] B. G. Penaflor, J. R. Ferron, A. W. Hyatt, M. L. Walker, R. D. Johnson, D. A. Piglowski, E. Kolemen, A. S. Welander, and M. J. Lanctot. Latest advancements in DIII-D Plasma Control software and hardware. *2013 IEEE 25th Symposium on Fusion Engineering, SOFE 2013*, pages 1–4, 2013.
- [4] M. Margo, B. Penaflor, H. Shen, J. Ferron, D. Piglowski, P. Nguyen, J. Rauch, M. Clement, A. Battey, and C. Rea. Current State of DIII-D Plasma Control System. *Fusion Engineering and Design*, 150(October 2019), 2020.
- [5] Mellanox Technologies. Introduction to InfiniBand. Technical report, 2003.
- [6] J. I. Paley, S. Coda, B. Duval, F. Felici, and J. M. Moret. Architecture and commissioning of the TCV distributed feedback control system. *Conference Record - 2010 17th IEEE-NPSS Real Time Conference, RT10*, pages 1–6, 2010.
- [7] H. Anand, C. Galperti, S. Coda, B. P. Duval, F. Felici, T. Blanken, E. Maljaars, J. M. Moret, O. Sauter, T. P. Goodman, and D. Kim. Distributed digital real-time control system for the TCV tokamak and its applications. *Nuclear Fusion*, 57(5), 2017.
- [8] A. C. Neto, F. Sartori, F. Piccolo, R. Vitelli, G. De Tommasi, L. Zabeo, A. Barbalace, H. Fernandes, D. F. Valcarcel, and A. J. N. Batista. Marte: A multiplatform real-time framework. *IEEE Transactions on Nuclear Science*, 57(2):479–486, April 2010.
- [9] G. De Tommasi, F. Piccolo, A. Pironti, and F. Sartori. A flexible software for real-time control in nuclear fusion experiments. *Control Engineering Practice*, 14(11):1387–1393, 2006.
- [10] André C. Neto, Diogo Alves, Luca Boncagni, Pedro J. Carvalho, Daniel F. Valcárcel, Antonio Barbalace, Gianmaria De Tommasi, Horácio Fernandes, Filippo Sartori, Enzo Vitale, Riccardo Vitelli, and Luca Zabeo. A survey of recent MARTe based systems. In *IEEE Transactions on Nuclear Science*, volume 58, pages 1482–1489, 2011.

Bibliography

- [11] A Neto, D Alves, B B Carvalho, P J Carvalho, H Fernandes, D F Valc, G De Tommasi, Associazione Euratom-enea create, Via Claudio, P McCullen, A Stephen, Euratom-ccfe Fusion Association, Culham Science Centre, Abingdon Ox, United Kingdom, R Vitelli, Tor Vergata, Via Politecnico, L Zabeo, and Iter Organisation. Marte Framework : a Middleware for Real-Time Applications Development. In *13th International Conference on Accelerator and Large Experimental Physics Control Systems*, number 11, pages 1277–1280, Grenoble, France, 2011.
- [12] Andre C. Neto, Filippo Sartori, Riccardo Vitelli, Llorenç Capella, Giuseppe Ferro, Ivan Herrero, and Hector Novella. An agile quality assurance framework for the development of fusion real-Time applications. In *2016 IEEE-NPSS Real Time Conference, RT 2016*, 2016.
- [13] Chiara Piron, Gabriele Manduchi, Paolo Bettini, Federico Felici, Claudio Finotti, Paolo Franz, Ondrej Kudlacek, Giuseppe Marchiori, Lionello Marrelli, J. M. Moret, Paolo Piovesan, Olivier Sauter, and Cesare Taliercio. Integration of the state observer RAPTOR in the real-time MARTE framework at RFX-mod. *Fusion Engineering and Design*, 123:616–619, 2017.
- [14] William R. Spears. JT-60SA construction status. *IEEE Transactions on Plasma Science*, 2014.
- [15] JT-60SA Team. Research objectives and strategy. Technical report, 2018. <http://www.jt60sa.org/>.
- [16] N Cruz, G. De Tommasi, M Mattei, A Mele, Y Miyata, A Pironti, and T Suzuki. Control-oriented tools for the design and validation of the JT-60SA magnetic control system. *Control Engineering Practice*, 63:81–90, 2017.
- [17] JT-60SA Team. Plant integration document. Technical report, 2017. <https://users.jt60sa.org/?uid=222UJY>.
- [18] R. Albanese, R. Ambrosino, and M. Mattei. CREATE-NL+: A robust control-oriented free boundary dynamic plasma equilibrium solver. *Fus. Eng. Des.*, 96–97:664–667, Oct. 2015.
- [19] R. Albanese and F. Villone. The linearized CREATE-L plasma response model for the control of current, position and shape in tokamaks. *Nucl. Fus.*, 38(5):723–738, May 1998.
- [20] R. Albanese, G. Ambrosino, M. Ariola, A. Cenedese, F. Crisanti, G. De Tommasi, M. Mattei, F. Piccolo, A. Pironti, F. Sartori, and F. Villone. Design, implementation and test of the XSC extreme shape controller in JET. *Fusion Engineering and Design*, 74(1-4):627–632, 2005.
- [21] H. Anand et al. A novel plasma position and shape controller for advanced configuration development on the TCV tokamak. *Nucl. Fus.*, 57(12):126026, 2017.
- [22] E. de la Luna et al. Recent Results on High-Triangularity H-Mode Studies in JET-ILW. In *26th IAEA Fusion Energy Conference*, Kyoto, Japan, October 2016.
- [23] G. Ambrosino et al. Design and Implementation of an Output Regulation Controller for the JET Tokamak. *IEEE Trans. Control Syst. Tech.*, 16(6):1101–1111, Nov. 2008.

- [24] M. Ariola and A. Pironti. The design of the eXtreme Shape Controller for the JET tokamak. *IEEE Control Sys. Mag.*, 25(5):65–75, Oct. 2005.
- [25] H. Urano et al. Y. Miyata. Documents on inputs, outputs of ccs(cauchy condition surface) method. Technical report, 2018.
- [26] H. Urano et al. Y. Miyata. Documents on inputs, outputs and control scheme of the qst magnetic controller. Technical report, 2018.
- [27] Y. Miyata et al. Study of JT-60SA Operation Scenario using a Plasma Equilibrium Control Simulator. *Plasma and Fus. Res.*, 8:2405109–2405109, 2013.
- [28] Y. Miyata, T. Suzuki, S. Ide, and H. Urano. Study of Plasma Equilibrium Control for JT-60SA using MECS. *Plasma and Fus. Res.*, 9:3403045–5, 2014.

A

EXTENDED CONTROL RESULTS

This appendix contains the corresponding plots of the ISTTOK discharges from table 5.2.1.

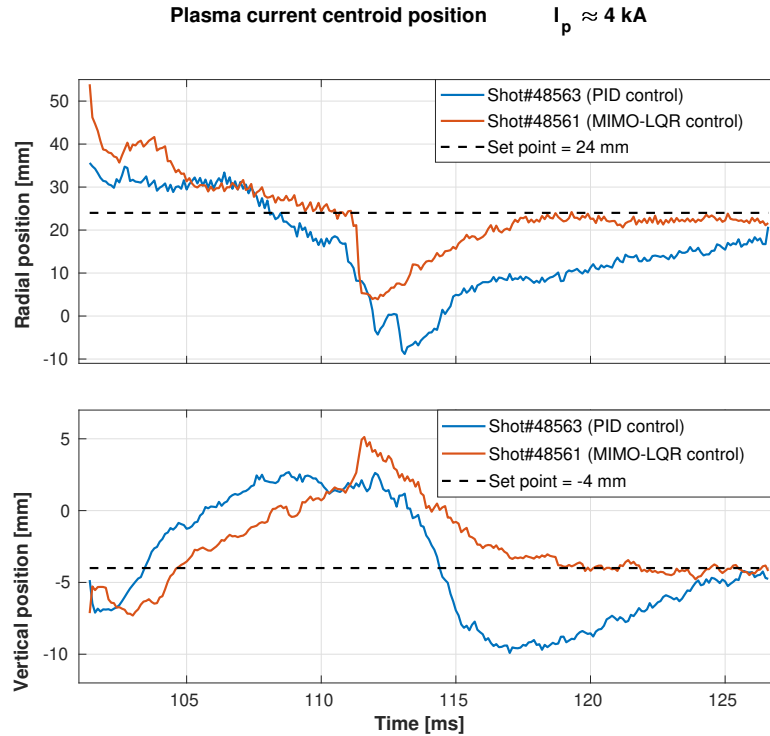


Figure A.1.: Plasma centroid position Shot# 48563 Shot# 48561

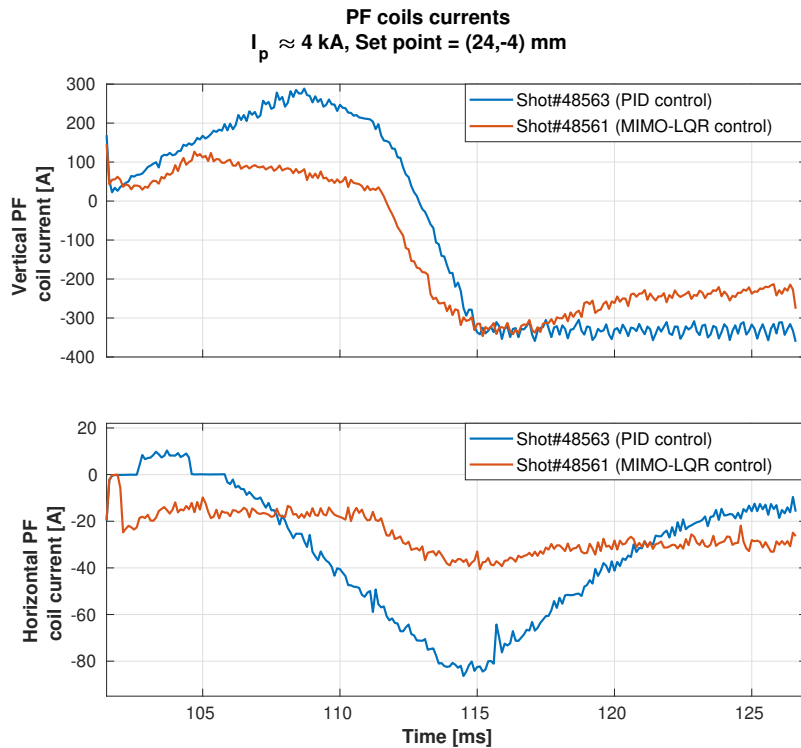


Figure A.2.: lalala Shot# 48563 Shot# 48561

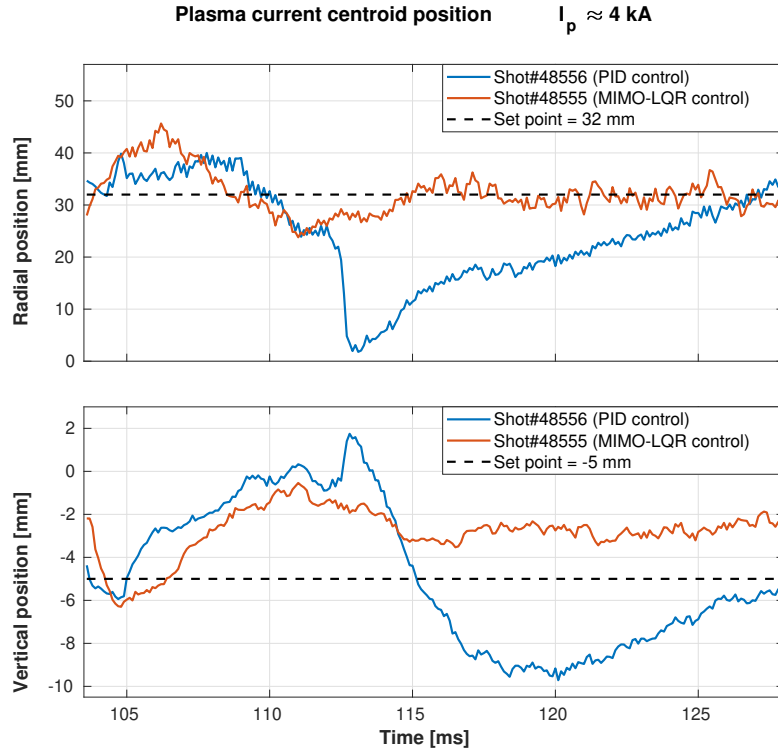


Figure A.3.: Plasma centroid position Shot# 48556 Shot# 48552

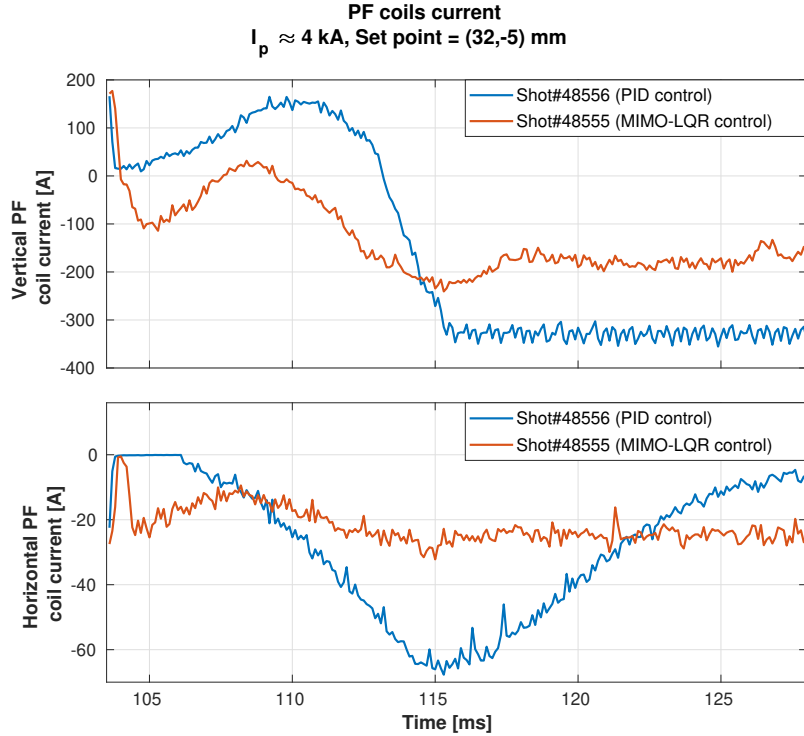


Figure A.4.: lalala Shot# 48556 Shot# 48552

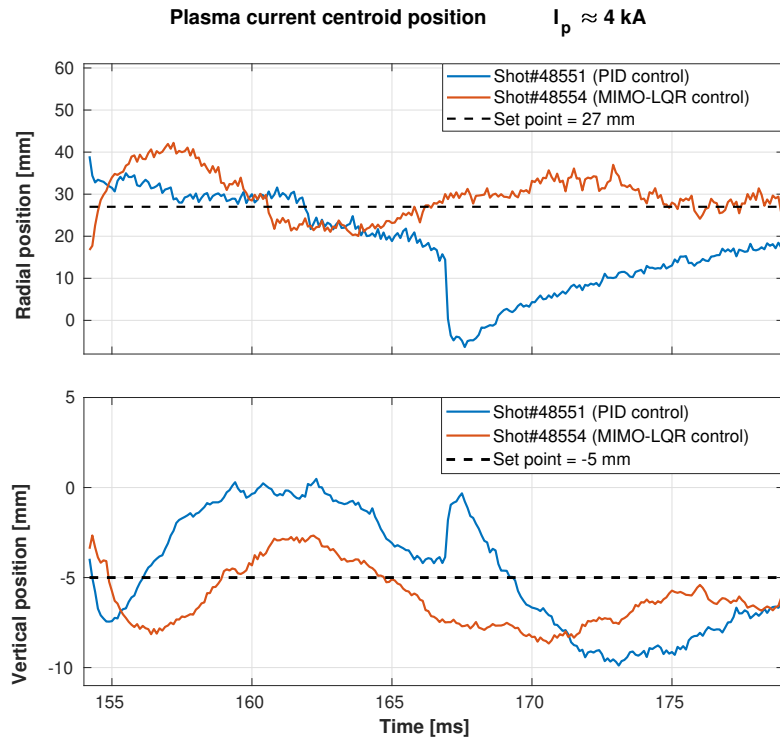


Figure A.5.: Plasma centroid position Shot# 48551 Shot# 48554

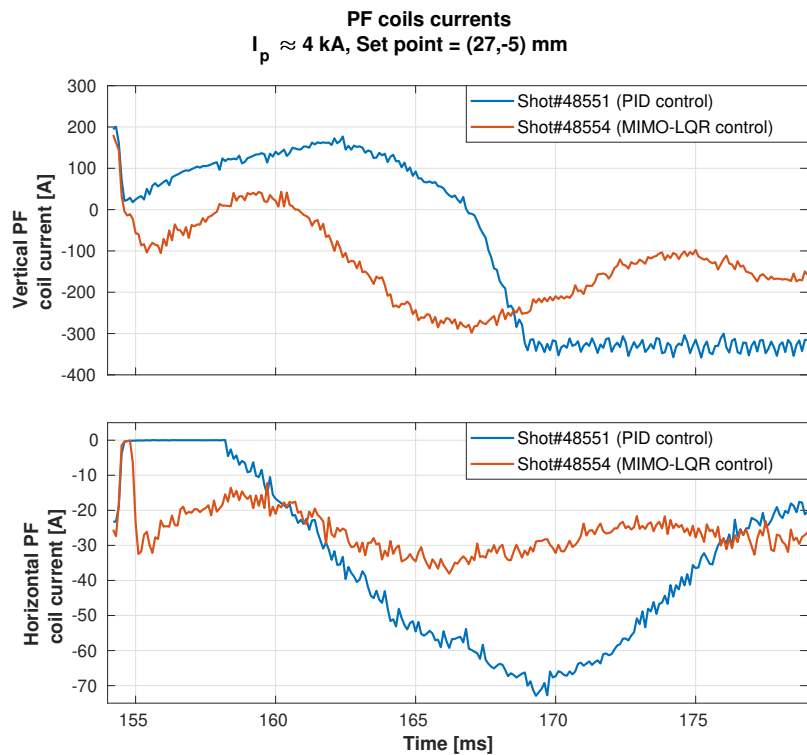


Figure A.6.: lalala Shot# 48551 Shot# 48554

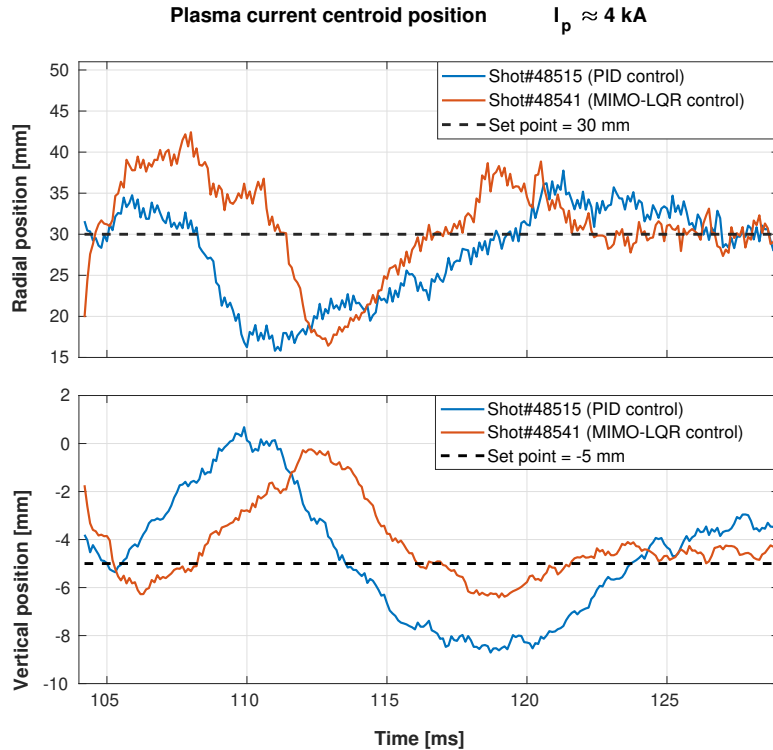


Figure A.7.: Plasma centroid position Shot# 48515 Shot# 48541

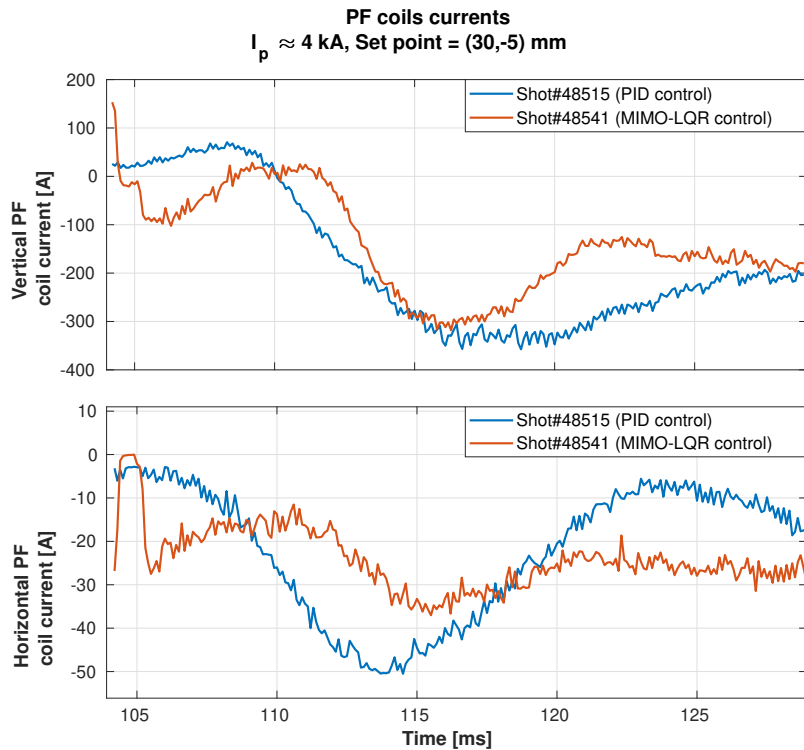


Figure A.8.: lalala Shot# 48515 Shot# 48541

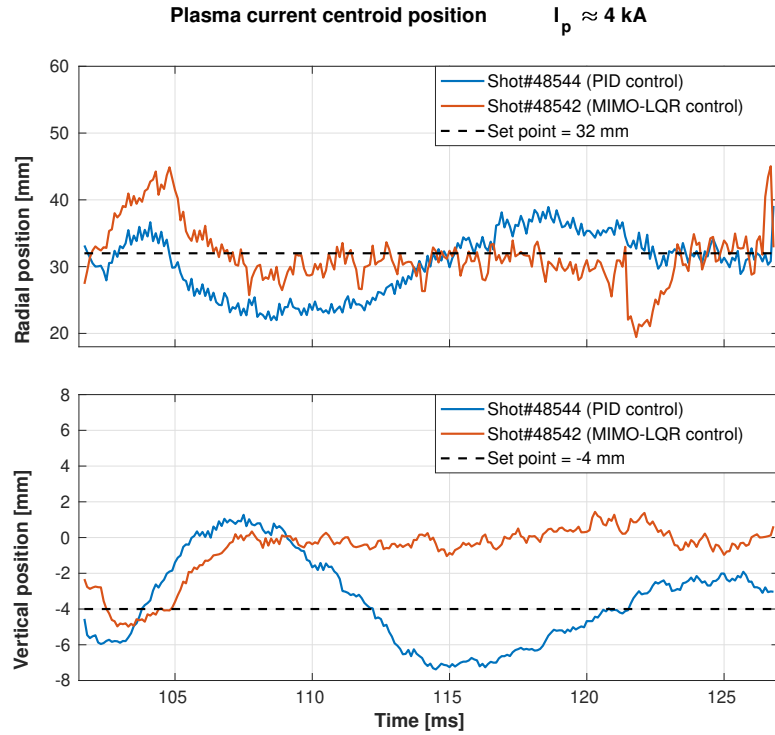


Figure A.9.: Plasma centroid position Shot# 48544 Shot# 48542

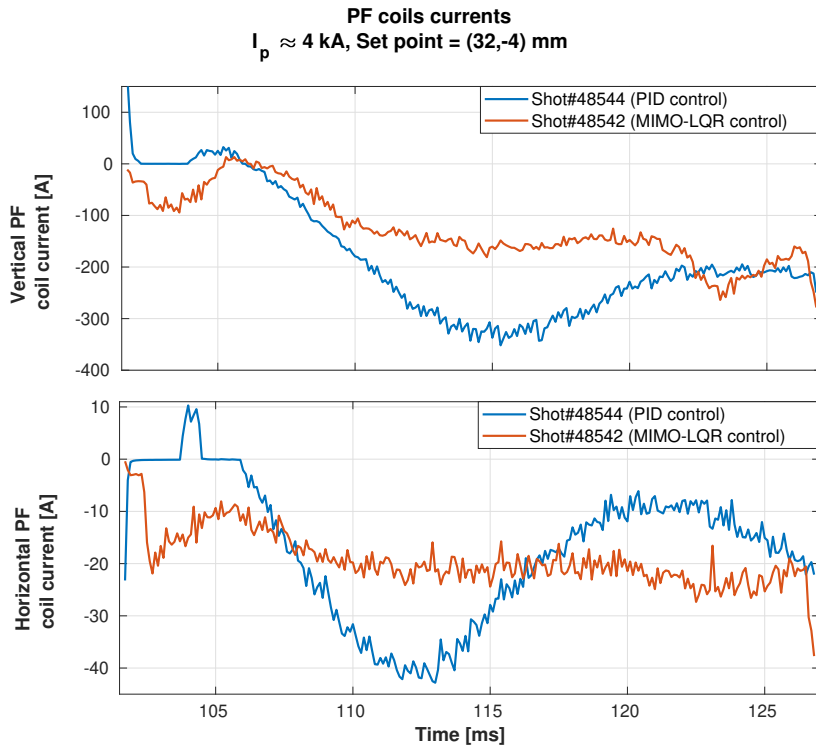


Figure A.10.: lalala Shot# 48544 Shot# 48542

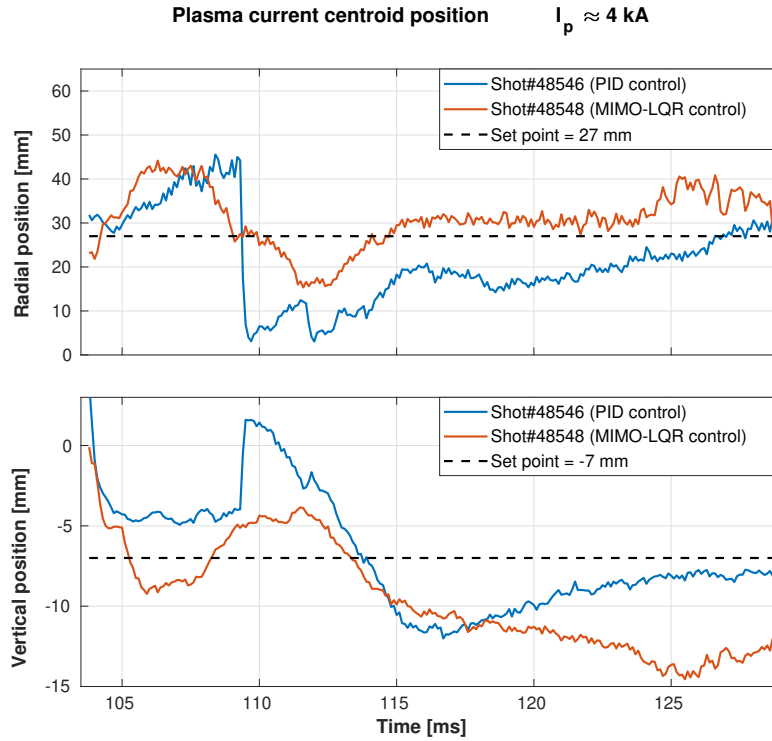


Figure A.11.: Plasma centroid position Shot# 48546 Shot# 48548

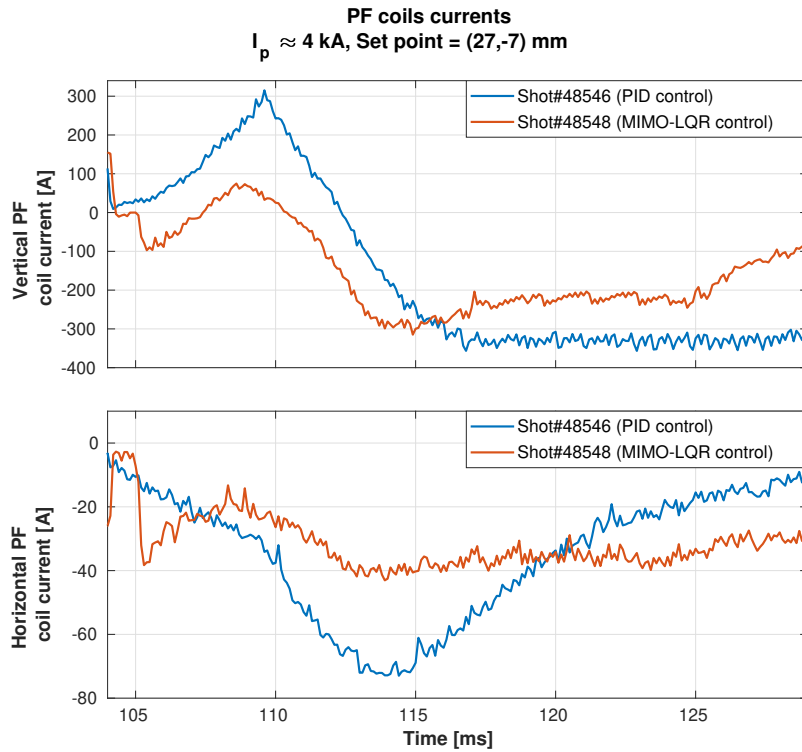


Figure A.12.: lalala Shot# 48546 Shot# 48548

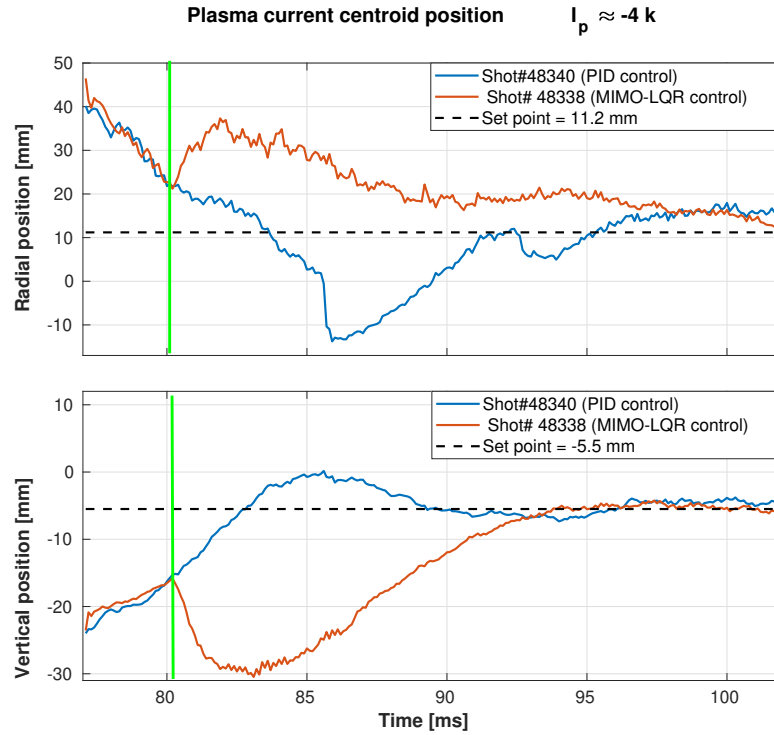


Figure A.13.: Plasma centroid position Shot# 48340 Shot# 48338

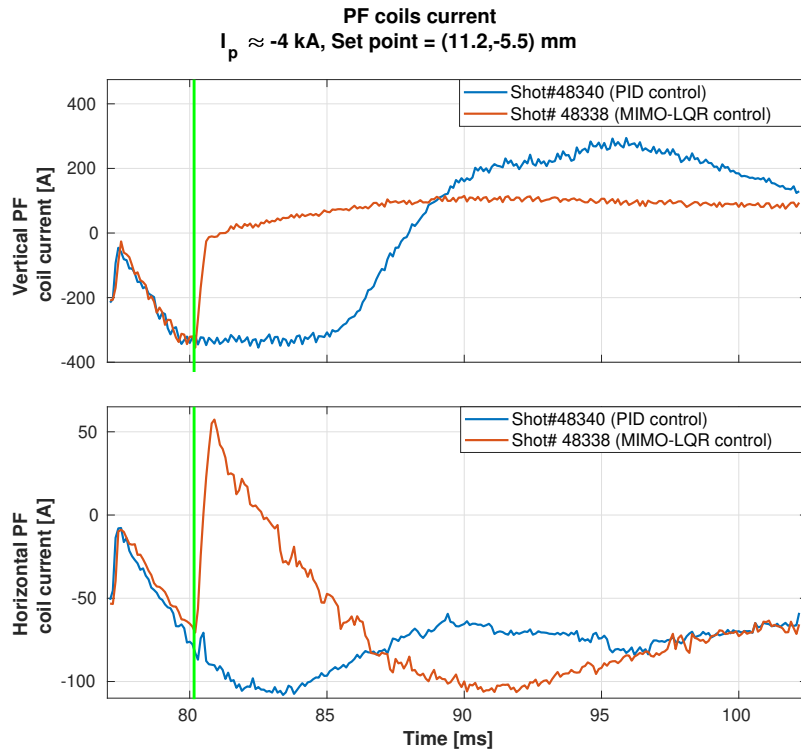


Figure A.14.: lalala Shot# 48340 Shot# 48338

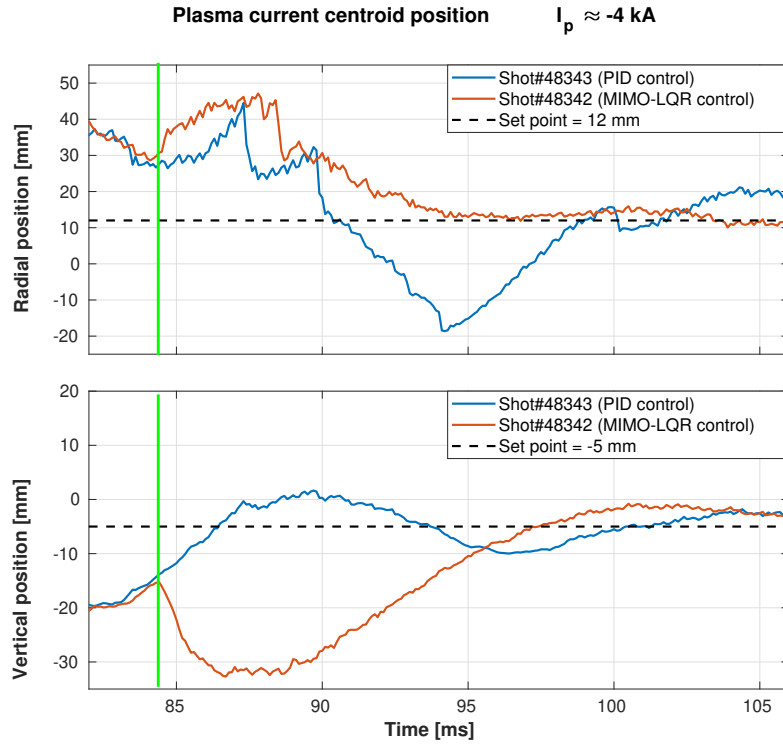


Figure A.15.: Plasma centroid position Shot# 48343 Shot# 48342

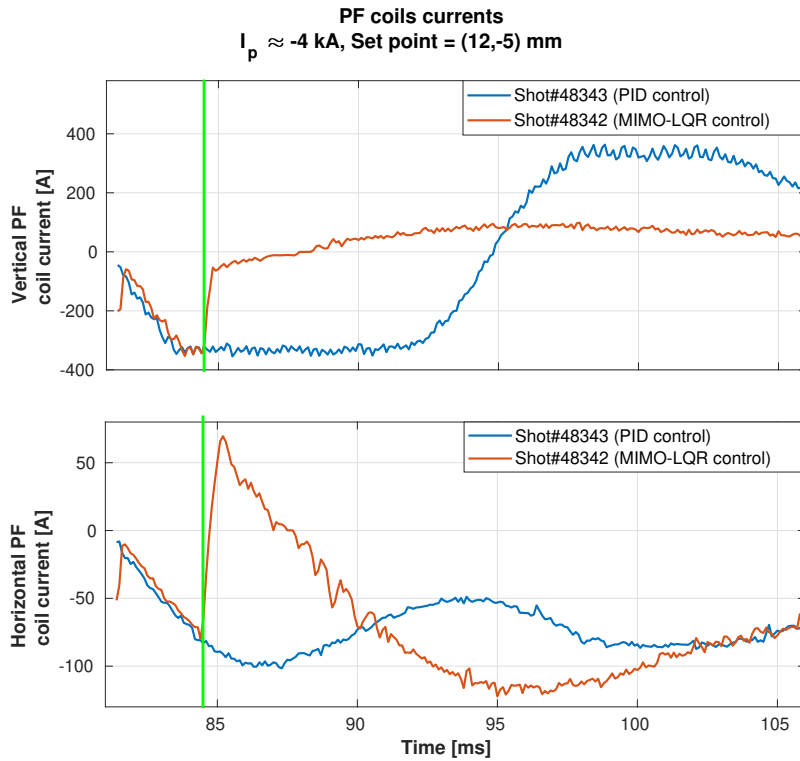


Figure A.16.: lalala Shot# 48343 Shot# 48342

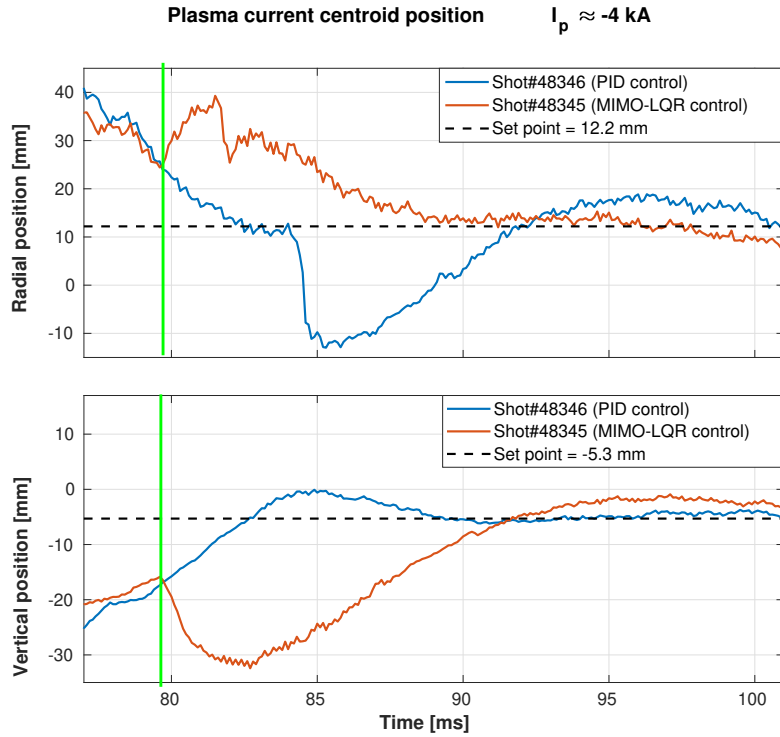


Figure A.17.: Plasma centroid position Shot# 48346 Shot# 48345

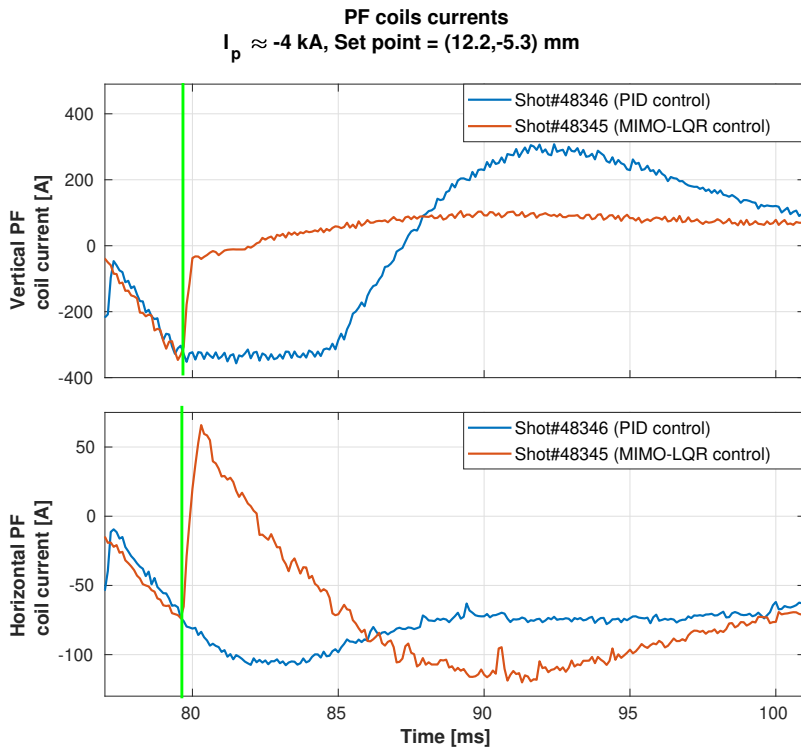


Figure A.18.: lalala Shot# 48346 Shot# 48345

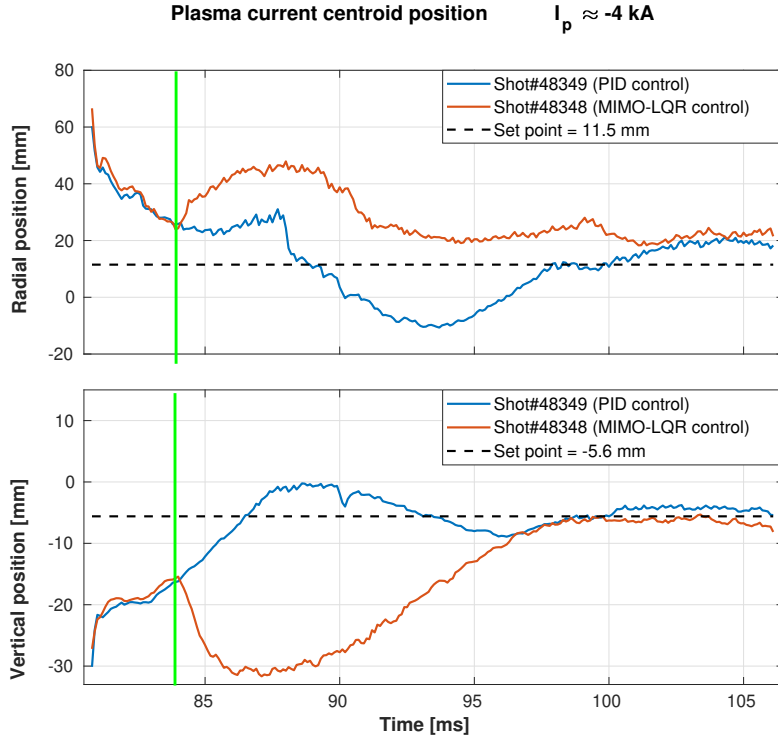


Figure A.19.: Plasma centroid position Shot# 48349 Shot# 48348

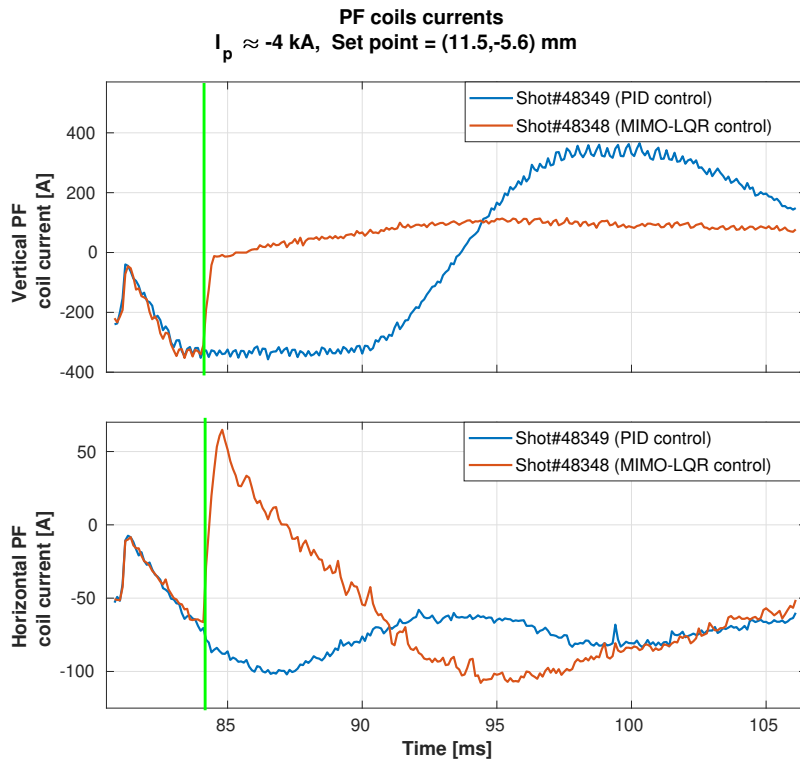


Figure A.20.: lalala Shot# 48349 Shot# 48348

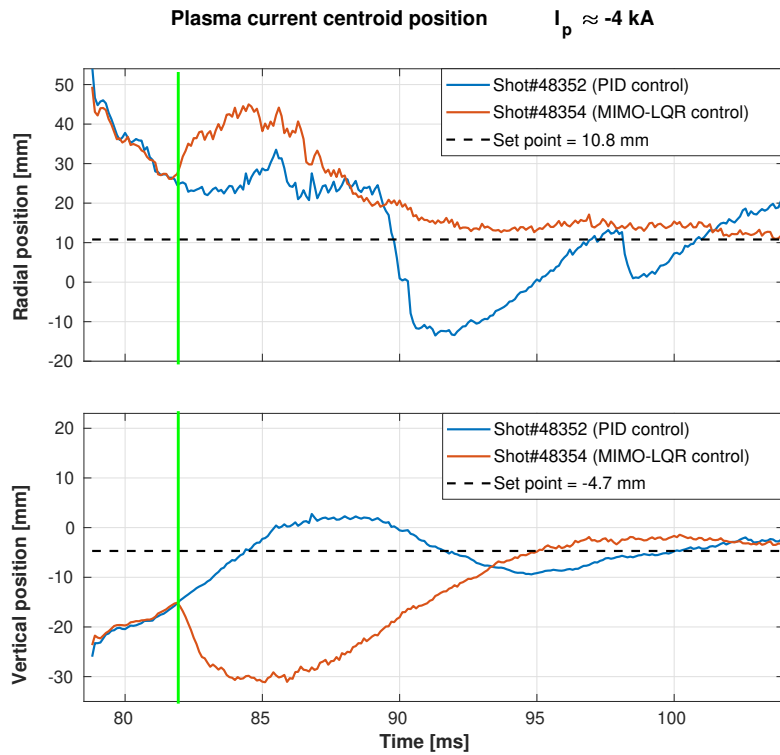


Figure A.21.: Plasma centroid position Shot# 48352 Shot# 48354

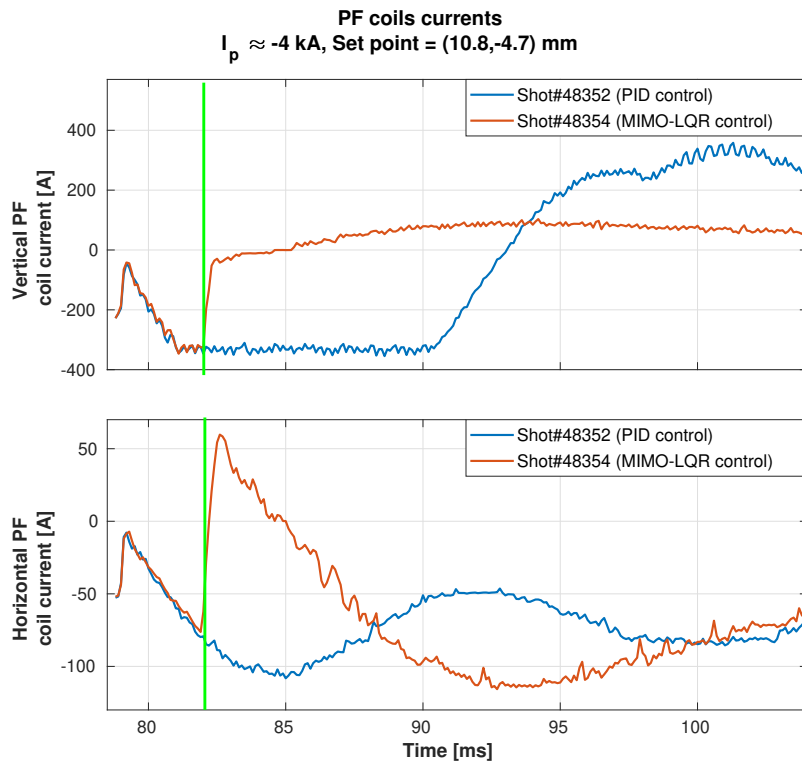


Figure A.22.: lalala Shot# 48352 Shot# 48354

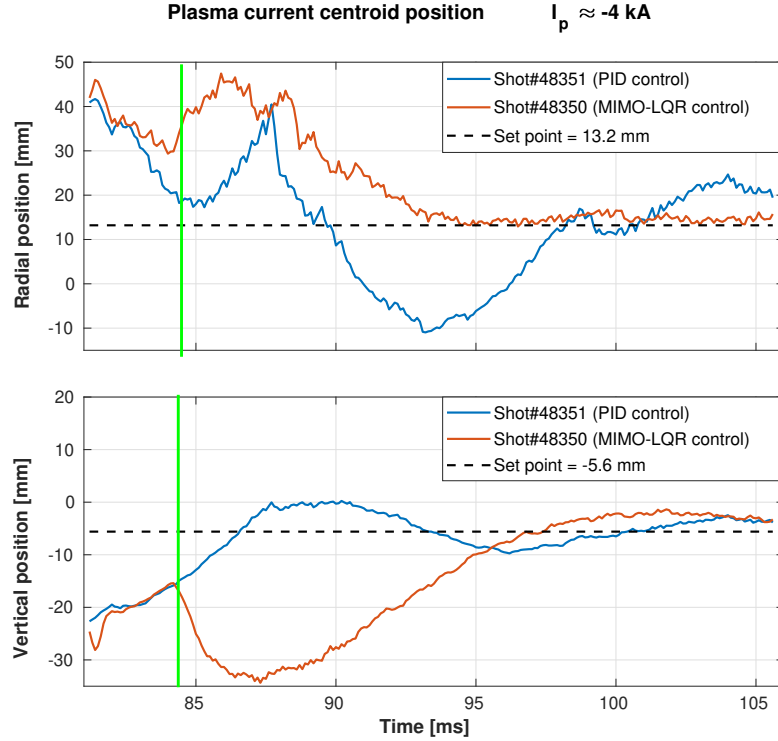


Figure A.23.: Plasma centroid position Shot# 48351 Shot# 48350

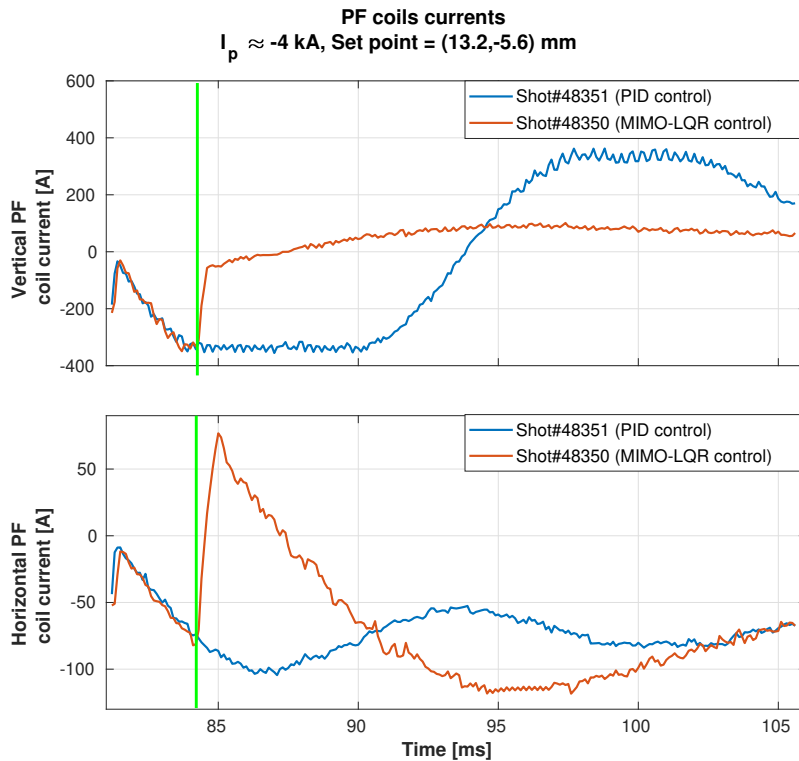


Figure A.24.: lalala Shot# 48351 Shot# 48350

B

FBC CONTROLLER AND CCS CONFIGURATION
